CHC22 clathrin initiates biogenesis of the human GLUT4 storage compartment from the early secretory pathway

Stéphane M. Camus[1,2,3,4,10], Marine D. Camus[1,2,3,4,10], Carmen Figueras-Novoa[10], L. Amanda Sadacca[10], Christopher Esk[5], Anne Bigot[6], Gwyn W. Gould[7], Dimitrios Kioumourtzoglou[8], Franck Perez[9,10], Nia J. Bryant[8], Shaeri Mukherjee[3,4*] and Frances M. Brodsky[1,2,3,4,11,*]

[1] Department of Bioengineering and Therapeutic Sciences,

[2] Department of Pharmaceutical Chemistry,

[3] Department of Microbiology and Immunology,

[4] The G.W. Hooper Foundation, University of California San Francisco, San Francisco, CA 94143, USA

[5] IMBA Institute of Molecular Biotechnology GmbH, Vienna, Austria

[6] Sorbonne Université, Inserm, Association Institut de Myologie, UMRS974 Centre for Research in Myology, F-75013 Paris, France

[7] Institute of Molecular, Cell and Systems Biology, College of Medical, Veterinary and Life Sciences, University of Glasgow, Glasgow, G12 8QQ, UK

[8] Department of Biology, University of York, York, YO10 5DD, UK

[9] Institut Curie, 26 rue d'Ulm, 75248 Paris, France.

[10] CNRS UMR 144, 26 rue d'Ulm, 75248 Paris, France.

[11] Present address: Division of Biosciences, University College London, London WC1E 6BT, UK

[*]Co-corresponding authors

Abstract

Glucose Transporter 4 (GLUT4) traffics from its intracellular storage compartment (GSC) to the cell surface to facilitate blood glucose uptake by muscle and fat, in response to insulin. Here we map the biosynthetic pathway for human GSC formation, which involves the clathrin isoform CHC22. We observe that GLUT4 transits more slowly through the early secretory pathway than the constitutively secreted GLUT1 transporter, and show that the GSC evolves from the endoplasmic-reticulum-to-Golgi-intermediate compartment (ERGIC). We find CHC22 is required to form the replication vacuole of *Legionella pneumophila* bacteria, which hijack ERGIC-derived vesicles, and show that the vacuole acquires components of the GLUT4 pathway. We show that p115 but not GM130 is required for GSC formation from the ERGIC, indicating Golgi bypass. This GSC biogenesis pathway is attenuated in mice, which lack CHC22 and rely mainly on recapture of surface GLUT4 to populate their GSC. In humans, GLUT4 traffic to the GSC is enhanced by CHC22 at the ERGIC, which has implications for pathways to insulin resistance.

Summary:

Blood glucose clearance relies on insulin-mediated exocytosis of glucose transporter 4 (GLUT4) from the GLUT4 storage compartment (GSC). Pathways to GSC formation are unknown. We show that CHC22 clathrin mediates GSC biogenesis from the ER-to-Golgi Intermediate Compartment in humans.

Glucose transporter 4 (GLUT4) mediates post-prandial blood glucose clearance into muscle and adipose tissues following insulin-stimulated translocation to the cell surface from an intracellular GLUT4 storage compartment (GSC) (Bogan, 2012; Leto and Saltiel, 2012). Deregulation of this process occurs during insulin resistance and contributes to pathogenesis of type 2 diabetes (T2D) (Bogan, 2012). In rodent models, endocytic pathways have been identified as essential routes for retrograde recycling of GLUT4 back to the GSC after insulin-mediated release (Antonescu et al., 2008; Bryant et al., 2002; Fazakerley et al., 2009; Jaldin-Fincati et al., 2017; Kandror and Pilch, 2011) but the trafficking routes leading to initial formation of the GSC are less well defined. In human myocytes and adipocytes, GSC formation involves the non-canonical isoform of clathrin, CHC22, which is missing from rodents due to loss of the encoding gene (Wakeham et al., 2005). Here we define a role for CHC22 clathrin in the biosynthetic trafficking pathway leading to initial GSC formation in humans.

The non-canonical clathrin isoform CHC22 is encoded on human chromosome 22 and has 85% sequence homology with the canonical CHC17 clathrin isoform (Wakeham et al., 2005). CHC17 performs receptor-mediated endocytosis at the plasma membrane and protein sorting at the *trans*-Golgi network in all eukaryotic cells and tissues (Brodsky, 2012). CHC22 has been implicated in distinct tissue-specific membrane traffic pathways consistent with its different biochemical properties and restricted tissue expression. While both CHC22 and CHC17 homo-trimerize into triskelia that assemble to form latticed vesicle coats, the CHC22 coat is more stable and within cells, the two clathrins form separate vesicles (Dannhauser et al., 2017). CHC22 does not bind the clathrin light chain subunits associated with CHC17 or the endocytic AP2 adaptor that recruits CHC17 to the plasma membrane, while CHC22 interacts preferentially with the GGA2 adaptor compared to CHC17 (Dannhauser et al., 2017; Liu et al., 2001; Vassilopoulos et al., 2009). In agreement

with its adaptor specificity, several analyses have now confirmed that CHC22 does not support receptor-mediated endocytosis at the plasma membrane (Dannhauser et al., 2017), though earlier studies suggested that it might replace CHC17 function upon over-expression (Hood and Royle, 2009).

In humans, CHC22 is expressed most highly in muscle, reaching about 10% of CHC17 levels, and has variable but lower expression in other tissues (Esk et al., 2010). In both human myocytes and adipocytes, CHC22 is needed for formation of the GSC, a membrane traffic pathway that these cell types uniquely share (Vassilopoulos et al., 2009). We previously observed that CHC22 is required for a retrograde transport pathway from endosomes (Esk et al., 2010), a step that CHC17 can also perform (Johannes and Popoff, 2008) and which has been shown to be important in murine GSC formation (Jaldin-Fincati et al., 2017). However, when CHC22 is depleted from human myocytes, CHC17 does not compensate for CHC22 loss and cells are still unable to form an insulin-responsive GSC, suggesting that CHC22 mediates an additional pathway in human GSC formation. CHC22 is also transiently expressed in the developing human brain (Nahorski et al., 2015) and has been implicated in protein targeting to dense core secretory granules, another pathway that involves sequestration of cargo away from standard endocytic and secretory pathways (Nahorski et al., 2018).

In the adipocytes and myocytes of insulin resistant type-2 diabetic patients, GLUT4 accumulates in an expanded GSC (Garvey et al., 1998; Maianu et al., 2001) where CHC22 also accumulates (Vassilopoulos et al., 2009). Transgenic expression of CHC22 in murine muscle caused similar accumulation of GLUT4 with CHC22 along with two other proteins involved in intracellular GLUT4 sorting, IRAP and VAMP2, and aged CHC22-transgenic animals developed hyperglycemia. These observations not only highlight fundamental differences in GLUT4 intracellular trafficking to the

GSC between human and mice, but also link abnormal CHC22 intracellular localization and function to defects in GLUT4 trafficking during insulin resistance. Therefore, mapping the CHC22-mediated GLUT4 trafficking pathways leading to the biogenesis of the GSC in humans is relevant to pathophysiology leading to type 2 diabetes. Understanding CHC22's role in GLUT4 traffic should also shed light on its role during the development of pain-sensing neurons, which was found to be defective in children homozygous for a rare familial mutation in the CHC22-encoding gene, who unfortunately did not survive to an age where their glucose metabolism could be studied (Nahorski et al., 2015).

In the present study, we identify the specialized pathway that CHC22 mediates during initial biogenesis of the human GSC by analyzing its trafficking in two independent cell models. We observed that CHC22 localizes to the early part of the secretory pathway where GLUT4 is delayed during its biogenesis relative to the constitutively secreted GLUT1 transporter. In particular, CHC22 colocalizes with the p115, a resident of the ER-to-Golgi Intermediate Compartment (ERGIC) where it participates in membrane export from that compartment. We confirmed that this compartment was ERGIC, by utilizing the bacterium *Legionella pneumophila* bacteria, which is known to co-opt membrane from the ERGIC to avoid the degradative environment of the endocytic pathway. Along with CHC22, the bacterial compartment also acquired essential components of the GLUT4 pathway, namely IRAP, sortilin and GGA2. We further found that the CHC22-dependent trafficking pathway for building the GSC relies on p115 but not GM130, indicating that initial GSC biogenesis in humans depends on diversion of newly synthesized GLUT4 directly from the ERGIC in an unconventional secretory route for intracellular sequestration.

Results

HeLa-GLUT4 cells have a functional GLUT4 trafficking pathway that requires CHC22.

To study the role of CHC22 in formation of the human GSC, we established a cellular model in which GLUT4 translocation can be easily detected. This was necessitated by limited experimental capacity of available human muscle and adipocyte cell lines and the widely acknowledged problem of detecting endogenous GLUT4 at the cell surface. We generated a stable HeLa cell line (HeLa-GLUT4) expressing human GLUT4 containing a haemagglutinin (HA) tag in the first exofacial loop and a GFP tag at the intracellular carboxyl terminus, a construct that has been extensively characterized and validated for the study of intracellular GLUT4 trafficking in rodent cells (Dawson et al., 2001; Dobson et al., 1996). HeLa cells were chosen because they have levels of CHC22 comparable to those in human muscle cells (Esk et al., 2010) and they also express sortilin, another protein important for formation of the GSC (Huang et al., 2013; Shi and Kandror, 2005; Shi and Kandror, 2007).

GLUT4 was sequestered intracellularly in HeLa-GLUT4 cells in the absence of insulin (basal), localized to both peripheral vesicles (arrowheads) and a perinuclear depot (arrows), as observed, respectively, for insulin-releasable GLUT4 vesicles and the tubulo-vesicular GSC of murine cells (Bryant et al., 2002; Shewan et al., 2003) (Fig. 1 A). Upon insulin treatment (15 min), GLUT4 was detected at the cell surface using a monoclonal antibody to the hemagglutinin (HA) tag (anti-HA) (Fig. 1 A). The degree of GLUT4 translocation was quantified using a fluorescence-activated cell sorter (FACS) to measure the mean fluorescence intensity of surface GLUT4 relative to the total GFP-GLUT4 (Fig. 1 B). Additionally, treatment of the HeLa-G4 cells with insulin induced phosphorylation of AKT and its substrate AS160, two modifications required for insulin-stimulated GLUT4 translocation (Bogan, 2012) (Fig. 1 C).

By structured-illumination microscopy (SIM), we observed that the perinuclear GLUT4 depot in HeLa-G4 cells partially co-localized with syntaxin-6 (STX-6) (arrowheads, Fig. 1 D), which is considered a marker of the GSC in rodent cells (3T3-L1 mouse adipocytes and L6 rat myotubes) (Foley and Klip, 2014; Shewan et al., 2003). In these models, GLUT4 released by insulin to the plasma membrane can return by endocytosis to the STX-6 –positive GSC within 30 minutes (Perera et al., 2003). Replicating this pulse-chase experiment in the HeLa-GLUT4 model, we labeled surface GLUT4 with anti-HA antibody following insulin stimulation and tracked internalized GLUT4 to a perinuclear compartment overlapping with STX-6 with similar kinetics to those observed in rodent cells (Fig. 1, E and F). The GSC formed in the HeLa-GLUT4 cells also had properties of the human GSC in that siRNA-mediated depletion of CHC22 induced dispersal of GLUT4 from the perinuclear region and inhibited insulin-stimulated GLUT4 translocation (Fig. 1, G and H) (Esk et al., 2010; Vassilopoulos et al., 2009). Taken together, our results show that HeLa cells stably expressing HA-GLUT4-GFP develop a functional GLUT4 trafficking pathway where insulin stimulation rapidly translocates GLUT4 to the plasma membrane, from where GLUT4 can be recycled back to the GSC. Further, CHC22 expression is critical for establishing this functional GLUT4 pathway. Thus, the model recapitulates features of the GSC observed for both mouse and human cells and can be used for analysis of pathways involved in GLUT4 trafficking in human cells. We note that during the course of this work, other laboratories developed and validated similar models of insulin-dependent GLUT4 translocation in HeLa cells (Haga et al., 2011; Trefely et al., 2015).

Newly synthesized GLUT4 co-localizes with CHC22 and is delayed in the early secretory pathway relative to constitutively expressed GLUT1.

Formation of the insulin-responsive GSC in rodent cells relies on the biosynthetic pathway feeding the GSC with newly synthesized GLUT4 (Watson et al., 2004), and

a recycling pathway that replenishes it after each round of insulin-mediated GLUT4 exocytosis (Antonescu et al., 2008; Bryant et al., 2002; Fazakerley et al., 2009; Kandror and Pilch, 2011; Martin et al., 2006). Our previous studies demonstrated a role for CHC22 in GSC formation (Vassilopoulos et al., 2009) and identified a function for CHC22 in retrograde transport from endosomes (Esk et al., 2010), suggesting that CHC22 could participate in GSC replenishment after GLUT4 translocation. To address whether CHC22 is also involved in GSC biogenesis from the secretory pathway, we tracked newly synthesized GLUT4 relative to CHC22 and other membrane traffic markers, using the Retention Using Streptavidin Hook (RUSH) approach (Boncompain et al., 2012). In this system, a streptavidin-binding protein (SBP) was inserted between GLUT4 and the GFP and the resulting fusion protein HA-GLUT4-SBP-GFP was co-expressed with streptavidin fused to an isoform of the human invariant chain of the major histocompatibility complex (Ii) that confers residency in the endoplasmic reticulum (ER)(Schutze et al., 1994). These transfected cells express HA-GLUT4-SBP-GFP that is retained in the ER but can be released synchronously to the cell surface upon addition of biotin to the cells. The HA-GLUT4-SBP-GFP was visualized relative to markers of the secretory pathway and CHC22 at different time points after biotin addition, and overlap was quantified. For comparison, we followed the intersection of HA-GLUT1-SBP-GFP with markers of the secretory pathway after biotin addition, as the secretion of GLUT1 is constitutive and it follows a conventional trafficking pathway to the plasma membrane (Hresko et al., 1994; Hudson et al., 1992). We observed that 30 minutes after biotin addition, GLUT1 had rapidly exited the ER and trafficked through the Golgi apparatus as exemplified by the 40% decrease in overlap with the ER resident protein calnexin (CNX) (Fig. 2, A and B; black line) and the transient increase in overlap with ERGIC markers (p115 and ERGIC53, Fig. 2 C-F; black lines), the Golgi marker GM130 and the trans-Golgi marker TGN46, Fig. 2, G-J; black lines). GLUT1 was detected at the plasma membrane as soon as 30 min post release (arrows) and by 60 minutes, GLUT1 was

detected in endosomal structures (arrowheads), indicating internalization from the plasma membrane. In contrast, GLUT4 exit from the ER was slower than GLUT1 (Fig. 2, A and B, red lines). GLUT4 overlap with ERGIC53, p115 and GM130 and TGN46 increased at 15 minutes post release but did not decrease over time (Fig. 2, C-J, red lines). That newly synthesized GLUT4 concentrates in a perinuclear region, localized with markers of the secretory pathway, is consistent with previous work in 3T3-L1 murine adipocytes showing that newly synthesized GLUT4 is diverted to the GSC before reaching the plasma membrane and subsequent endosomal compartments (Watson et al., 2004). GLUT4 co-localization with CHC22 was similar to its residence with secretory pathway markers, peaking at 15 minutes but remaining more co-localized with CHC22 than GLUT1, which only transiently overlapped with CHC22 (Fig. 2 K). Overall, this experiment indicates that the trafficking kinetics of newly synthesized GLUT1 and GLUT4 are fundamentally different, suggesting different trafficking routes and confirming previous observations (Hresko et al., 1994; Hudson et al., 1992). Moreover, GLUT4, and not GLUT1, was retained in a perinuclear region that overlaps with CHC22, suggesting a role for CHC22 in trafficking newly synthesized GLUT4 and that CHC22 might interact with secretory pathway compartments.

CHC22 localizes with markers of the ER-to-Golgi Intermediate Compartment.

To identify potential locations for CHC22 function in transporting newly synthesized GLUT4, we analyzed CHC22 overlap with markers of the secretory pathway in HeLa-GLUT4 cells and in several differentiated human myotubes cell lines. Using a new polyclonal antibody specific for CHC22 and not reactive with CHC17 (Fig. S1 A), we observed significant co-localization of CHC22 and two markers of the ERGIC, namely p115 (Alvarez et al., 2001) and ERGIC-53 (Lahtinen et al., 1996) (Figs. 3 A and S1 B and C), while there was only partial overlap with Golgi markers GM130 and TGN46 (Figs. 3 A and S1 D and E) and no significant co-localization of CHC22 with

endoplasmic reticulum (ER) markers or calreticulin or calnexin (Figs. 3 A and S1 F and G). Given the limited spatial resolution of conventional laser scanning confocal microscopy (200 nm), these overlap values could be overestimated. We therefore used super-resolution Structured Illumination Microscopy (SIM), which improves lateral resolution twofold (100 nm). Using SIM, we confirmed the substantial overlap between CHC22 and ERGIC markers in HeLa GLUT4 and human skeletal muscle cells (Figs. 3 B-D, arrowheads, and S1 I). SIM analysis did not support the apparent overlap between CHC22 and Golgi markers obtained by confocal microscopy. In fact, CHC22 was separated from the cis-Golgi and trans-Golgi markers GM130 (Figs. 3 E and S1 I) and TGN46 (Figs. 3 F and S1 H and I), respectively.

If the intersection of GLUT4, CHC22 and the ERGIC markers represents a GSC-formation pathway, GLUT4 internalized from the plasma membrane after release should be localized near these markers. Indeed, when GLUT4 uptake was tracked following insulin stimulation, internalized GLUT4 showed time-dependent co-localization with CHC22 and ERGIC53 (Fig. S2 A-D) after 10 and 30 minutes of re-uptake, indicating that the GSC, where recaptured GLUT4 accumulates, is located in close proximity to CHC22 and the ERGIC. Furthermore, when we treated HeLa GLUT4 or human myotubes with Brefeldin A (BFA), CHC22 co-distributed with the ERGIC marker p115 and segregated away from the persisting GSC (Fig. S3 A and B). This is consistent with our previous observations that BFA does not cause CHC22 to dissociate from intracellular membranes (Liu et al., 2001) and supports association of CHC22 with ERGIC membranes. This also supports observations from others showing that the GSC is not affected by BFA (Martin et al., 2000). Together, these data suggest that CHC22 is not a final component of the stable GSC, but could be involved in initial GSC formation from the secretory pathway by mediating GLUT4 trafficking from the ERGIC to the GSC.

CHC22 participates in membrane trafficking from the ERGIC.

To establish whether CHC22 has functional activity at the ERGIC, we took advantage of *Legionella pneumophila* (*L.p.*), a facultative intracellular pathogen that avoids the host's endo-lysosomal compartment and specifically hijacks membranes from the early secretory pathway to create an ER/ERGIC-like, *L.p.*-containing vacuole (LCV) for replication (Kagan and Roy, 2002). Upon infection, *L.p.* secretes ~300 effector proteins, through a type IV secretion system, some of which enable recruitment of ER / ERGIC proteins calnexin, Sec22b, Rab1, ERGIC-53 and Arf1 to the LCV (Derre and Isberg, 2004; Kagan and Roy, 2002; Kagan et al., 2004), which are needed for its replication. The mature LCV retains ER-like properties, including the lumenal proteins calnexin, BiP and calreticulin and does not acquire Golgi markers (Derre and Isberg, 2004; Kagan and Roy, 2002; Kagan et al., 2004; Treacy-Abarca and Mukherjee, 2015). Given that the LCV is derived from the ER, and that CHC22 localizes to a compartment emerging from the ER, we tested whether CHC22 associates with membranes involved in LCV formation by transient expression of GFP-tagged CHC22 or GFP-tagged CHC17 in A549 human lung adenocarcinoma cells followed by *L.p.* infection. CHC22, but not CHC17, was associated with the membranes surrounding the LCV (Fig. 4 A and B). Similar LCV co-localization with CHC22 was observed in untransfected cells infected with *L.p.* and immuno-stained for endogenous CHC22 or CHC17 (Fig. 4 C). CHC22 did not localize with the isogenic avirulent *L.p.* mutant *ΔdotA,* which still enters cells but lacks a functional secretion system and cannot secrete effectors to create an ER-like vacuole (Fig. 4 A and B). To further address whether CHC22 is involved in transfer of membrane to the LCV, we treated A549 cells with siRNA targeting CHC22 prior to infection. The resulting CHC22 down-regulation significantly compromised recruitment of Sec22b to the bacterial vacuole at 1 hour post-infection (Fig. S4 A and B), suggesting defective vacuole maturation. This was confirmed by assessing bacterial replication eight hours after infection with WT or *ΔdotA L.p.* strains following

CHC22 or CHC17 silencing. CHC22 silencing reduced the proportion of vacuoles containing >4 *L.p.* by more than 9-fold, while CHC17 silencing reduced vacuoles with >4 *L.p.* by only 2-fold (Fig. 4 D), indicating that CHC22 is required to form a replicative vacuole and a possible role for CHC17 during bacterial uptake. The latter conclusion is supported by the observation that after CHC22 down-regulation, vacuoles with 1 *L.p.*, indicating bacterial entry, were observed, but vacuoles with 1 *L.p.* were less frequent in cells silenced for CHC17 infected with an equivalent number of bacteria. Infection of cells transfected with siRNA targeting CHC22 with an equivalent number of avirulent *ΔdotA L.p.* showed that these bacteria could also enter cells, with 94% vacuoles observed harboring only 1 *L.p.* (Fig. 4 D). These observations indicate that *L.p.* specifically co-opts CHC22 to acquire membrane derived from the early secretory pathway, which is needed for maturation of a replication-competent LCV, and suggest that *L.p.* effectors might interact with CHC22 or its partners.

Since CHC22-mediated membrane traffic contributes to formation of the LCV, we addressed whether GLUT4 or other components of the GLUT4 trafficking pathway traffic to the LCV. After infection, we observed significant enrichment of IRAP, sortilin and GGA2 to the LCV, all known functional partners for GLUT4 during membrane traffic to the GSC (Li and Kandror, 2005; Shi et al., 2008; Shi and Kandror, 2005; Shi and Kandror, 2007; Watson et al., 2004) (Fig. 5 A-F). We also observed host Rab1, a host protein that is recruited to the LCV and extensively modified (Mukherjee et al., 2011) (Fig. 5 A and F). In contrast, the localization of GLUT4 (Fig 5A and Fig S4 C) or Sec16a (Fig. S4 D, E) on the LCV was not statistically significant (Figs. 5 A and S4 D and E). We also did not detect p115 on the LCV, confirming previous work from others and suggesting that one of the *L.p.* effectors is a p115 substitute (Derre and Isberg, 2004) (Fig. 5 A and B). *L.p.* has bacterial effectors such as LidA that can bind to Rab1 and possibly substitute the function of p115 (Machner and Isberg, 2006).

Thus, analysis of *L.p.* infection indicates that CHC22 actively traffics membranes from the early secretory pathway to the LCV, and that this pathway also traffics a subset of proteins involved in forming the GSC.

CHC22 interacts with p115 and each influences stability of different partners for GLUT4 membrane traffic.

Previous work implicated the vesicle tether p115 in murine GSC formation in 3T3-L1 adipocytes by showing an interaction between p115 and IRAP and demonstrating that expression of the interacting fragment of p115 had a dominant negative effect on the GLUT4 insulin response (Hosaka et al., 2005). Given the high degree of co-localization between CHC22 and p115, we addressed the possibility that CHC22 and p115 might also associate. Endogenous CHC22 or CHC17 were immunoprecipitated from lysate of HeLa-GLUT4 and p115 co-precipitated with CHC22 but not CHC17 (Fig. 6 A). An association between p115 and CHC22 was also detected in lysate of human skeletal muscle myotubes (Fig. 6 B). To explore the possibility that p115 might be a link between CHC22 and components of the GLUT4 pathway, we assessed the effect of CHC22 and p115 silencing on each other and on other potential partner proteins involved in GLUT4 traffic. In particular, we focused on the fate of IRAP, sortilin and GGA2. These proteins were all found associated with the LCV (Fig. 5 A and C-E) and all three have been implicated in rodent GSC formation (Li and Kandror, 2005; Shi et al., 2008; Shi and Kandror, 2005; Shi and Kandror, 2007; Watson et al., 2004). Furthermore, IRAP co-localizes with CHC22 (Fig S5 A) (Vassilopoulos et al., 2009), GGA2 is enriched in CHC22-coated vesicles (Dannhauser et al., 2017; Vassilopoulos et al., 2009) and direct binding interactions between GLUT4, IRAP, sortilin and GGA2 have been described (Li and Kandror, 2005; Shi et al., 2008; Shi and Kandror, 2005; Shi and Kandror, 2007; Watson et al., 2004). CHC22 silencing destabilized GLUT4, sortilin and GGA2 while p115 and IRAP remained unchanged (Fig. 6 C, D and G). Conversely, p115 depletion destabilized

IRAP (Fig. 6 D, E and H) but none of the other components. None of the GLUT4 trafficking components were destabilized upon CHC17 depletion (Fig. 6 C, D, E and F), which, as previously observed (Dannhauser et al., 2017; Esk et al., 2010; Vassilopoulos et al., 2009), stabilized CHC22, likely due to increased membrane association as a result of reduced competition for shared adaptors such as GGA2 and AP1. Together these experiments suggest that CHC22, p115, GGA2 and sortilin interact with each other and could cooperate early in the secretory pathway for GLUT4 diversion to the GSC.

Membrane traffic to the human GSC requires CHC22 and p115, but not GM130.

To investigate the involvement of the early secretory pathway in human GSC formation, we depleted CHC22, p115 or the *cis*-Golgi tether protein GM130 from HeLa-GLUT4 cells using siRNA (Fig. 7 A) and assessed the morphology of the GSC by confocal microscopy (Fig. 7 B and C). Silencing of p115 or of CHC22 caused GLUT4 dispersion in the cell periphery, with down-regulation of one affecting the distribution of the other (Fig. 7 B). We did not detect any impact of GM130 depletion on GLUT4 subcellular distribution, though GM130 depletion did partially alter p115 distribution (Fig. 7 C).

Next, we evaluated the effect of CHC22, p115 or GM130 depletion on insulin-induced GLUT4 translocation, as assessed by FACS analysis of HeLa-G4 cells. Insulin-stimulated GLUT4 translocation was lost from cells silenced for p115 or CHC22 while CHC17 silencing had a partial effect on GLUT4 translocation (Fig. 7 D), consistent with previous observations for CHC22 and CHC17 down-regulation (Vassilopoulos et al., 2009). Notably, however, GM130 depletion, functionally confirmed by reduction of alkaline phosphatase secretion (Tokumitsu and Fishman, 1983) (Fig. S5 B), did not abrogate insulin-stimulated GLUT4 translocation (Fig. 7 D), suggesting that the trafficking pathway mediated by CHC22 and p115 leading to

GSC biosynthesis is independent of GM130. These results further indicate that both CHC22 or p115 are essential for GLUT4 trafficking to the human GSC and that the human GSC forms from the early secretory pathway and bypasses the Golgi such that GM130 is not required for GSC formation.

Discussion

CHC22 clathrin is required for formation of the insulin-responsive GLUT4 storage compartment (GSC) in human muscle and fat (Esk et al., 2010; Vassilopoulos et al., 2009) and has been implicated in specialized membrane traffic to dense core granules in neuronal cells (Nahorski et al., 2018). Both of these roles require diversion of intracellular cargo into privileged storage compartments so that the cargo is sequestered from degradation. Previous studies indicated a role for CHC22 clathrin in retrograde transport from endosomes (Esk et al., 2010), where CHC17 has been implicated in returning released GLUT4 to the GSC in murine cells (Gillingham et al., 1999; Li and Kandror, 2005). However, depletion of CHC22 from human muscle cells abrogates GSC formation even in the presence of CHC17 (Vassilopoulos et al., 2009), so we suspected a second pathway for CHC22 function in GLUT4 transport unique to this isoform of clathrin. We focused on pathways that would be involved in biosynthetic formation of the GSC, as it is known that GLUT4 arrives at the GSC prior to its expression on the plasma membrane (Watson et al., 2004). Discovering strong co-localization of CHC22 with the ERGIC markers p115 and ERGIC53, we investigated a role for CHC22 in formation of the replication vacuole of *Legionella pneumophila* (*L.p.*), which acquires membrane from the early secretory pathway to evade degradative compartments (Derre and Isberg, 2004; Kagan and Roy, 2002). We found that CHC22 was required for bacterial replication and formation of the *L.p.*-containing vacuole (LCV), and that components of the GLUT4 trafficking pathway localized to the LCV, though the presence of GLUT4 itself was highly variable. A difference between LCV and GSC formation is a requirement

for cellular p115. We showed that p115 was needed for human GSC formation, and it has previously been implicated in murine GSC formation (Hosaka et al., 2005), but *L.p.* bacteria have an effector protein that replaces p115 (Machner and Isberg, 2006). We therefore suggest that p115 is needed specifically to enable CHC22 to divert GLUT4 from the ERGIC to the GSC, but otherwise the formation of the GSC is similar to that of the LCV with both emerging from the early secretory pathway. Consistent with this mapping of GSC biogenesis, we found that GLUT4 newly released from the endoplasmic reticulum (ER) (using the RUSH system) resides for a longer period of time with markers of the early secretory pathway compared to the behavior of constitutively secreted GLUT1 after its release from the ER. We also found that while formation of the human GSC is sensitive to depletion of p115 and CHC22, GSC formation is not affected by depletion of GM130, supporting a Golgi bypass during GSC biogenesis. This proposed pathway is also consistent with previous reports of slower transit time for GLUT4 to the cell surface compared to GLUT1 and with the fact that maturation of carbohydrate side chains on GLUT4 is also many hours slower (Hresko et al., 1994; Hudson et al., 1992). Delayed modification of GLUT4 carbohydrate could be explained by diversion of most newly synthesized GLUT4 to the GSC from the ERGIC, followed by a process of carbohydrate maturation that depends on GLUT4 secretion and recapture through a retrograde pathway (Shewan et al., 2003) where low-level carbohydrate modification can occur by Golgi enzymes being recycled to their home compartments (Fisher and Ungar, 2016). In humans and even in CHC22 transgenic mice, CHC22 expression parallels that of GLUT4, with its highest expression in GLUT4-expressing tissues (Hoshino et al., 2013). However, unlike the tight regulation of GLUT4 expression, CHC22 is expressed at low levels in additional cell types (Nahorski et al., 2015). Thus, the CHC22 sorting pathway emerging from the ERGIC that we define here and CHC22-mediated retrograde sorting may also operate in tissues that do not express

GLUT4, albeit at a low level to target yet-unidentified cargo to specialized organelles, avoiding the conventional secretory or endocytic pathways.

Our demonstration that CHC22 functions in transport from the early secretory pathway defines a membrane traffic step in which the canonical CHC17 clathrin is not involved (Brodsky, 2012). We show that CHC22 co-immunoprecipitates with p115 and that CHC17 does not, indicating that the two clathrins form distinct complexes, consistent with previous findings that they localize to distinct cellular regions (Liu et al., 2001) and form distinct coated vesicles (Dannhauser et al., 2017). It was previously shown that p115 interacts with IRAP (Hosaka et al., 2005), a protein that binds GLUT4 and is co-sequestered in the GSC (Shi et al., 2008) and that expression of a p115 fragment prevents GSC formation (Hosaka et al., 2005). Furthermore, we show here that p115 downregulation reduces the stability of IRAP. Thus, we propose that the p115-IRAP interaction that would occur in the ERGIC after IRAP emerges from the ER stabilizes IRAP and triggers the coalescence of a protein domain that promotes sorting of GLUT4 to the GSC by binding GLUT4 and recruiting additional components (Fig. 8). In addition to interacting with each other, IRAP and GLUT4 both interact with sortilin (Shi and Kandror, 2005; Shi and Kandror, 2007), which in turn binds GGA2 (Li and Kandror, 2005; Nielsen et al., 2001), providing a platform for CHC22 recruitment and assembly, leading to GLUT4 sequestration. Accordingly, a GGA requirement for GSC formation has been previously demonstrated (Li and Kandror, 2005; Watson et al., 2004) and GGA2 shows preferential binding to CHC22 over CHC17 (Dannhauser et al., 2017; Vassilopoulos et al., 2009). Recruitment of GGA2 via sortilin would bypass the need for ARF1-mediated GGA2 recruitment (Puertollano et al., 2001), which is consistent with the CHC22 coat (and the GSC) being insensitive to Brefeldin A (Fig. S3) (Liu et al., 2001; Martin et al., 2000), which dissociates ARF1 from membranes (Niu et al., 2005). In summary, our model proposes that when IRAP meets p115 in the ERGIC, IRAP is

stabilized, which allows coalescence of a protein domain that includes IRAP, GLUT4 and sortilin, which then recruits GGA2 and CHC22 for sorting to the GSC. This domain may form less well during sorting to the *L.p.* LCV, if the bacterial equivalent of p115 does not stabilize IRAP as effectively, accounting for variable incorporation of GLUT4 into the LCV.

Identification of this sorting pathway for GLUT4 from the ERGIC to the GSC adds to the variety of sorting pathways that are known to emerge from the ERGIC, sustaining both conventional (ER-to-Golgi) (Kondylis and Rabouille, 2003; Sohda et al., 2007) and unconventional (Golgi bypass) pathways for autophagy (Ge et al., 2013; Ge and Schekman, 2014) or cargo exocytosis (Piao et al., 2017). Furthermore, our model for GLUT4 sorting to the GSC from the ERGIC is consistent with the reported ERGIC localization of the TUG protein involved in GLUT4 vesicle retention (Orme and Bogan, 2012) and with the recent finding that Sec16A is required for GSC formation. Sec16A was found to be a target for Rab10 (Bruno et al., 2016), which is activated by insulin-induced phosphorylation of AS160 (Larance et al., 2005; Sano et al., 2007) and Sec16A participates in GLUT4 membrane traffic independently of its conventional COPII partners (Bruno et al., 2016). The documented interaction of Sec16A with p115 (van Zuylen et al., 2012), as well as its presence at ER exit sites, suggests that Sec16A could be captured from the ERGIC during the pathway of GSC formation suggested here.

GLUT4 membrane traffic has primarily been studied using murine adipocyte and rat myoblast cell lines, which do not express CHC22 as a result of gene loss in the rodent lineage (Wakeham et al., 2005). Such studies have established that the major pathway for targeting GLUT4 to the GSC in rodent cells relies on retrograde transport of GLUT4, via endosomal-TGN sorting, after its release to the cell surface from the GSC and uptake by CHC17 (Bryant et al., 2002; Jaldin-Fincati et al., 2017). Our

studies here (Fig. 1) support the existence of this retrograde pathway in human cells. It is also reported that in rodent cells GLUT4 reaches the GSC prior to its insulin-stimulated release to the cell surface (Lamb et al., 2010; Watson et al., 2004), and in rodent cells there is involvement of p115 (Hosaka et al., 2005). Thus, the pathways that lead to GSC formation in humans and rodents appear to be the same, but the balance of their contribution to GSC formation is different. In rodent cells, GLUT4, IRAP, p115, sortilin and possibly Sec16A can coalesce in the ERGIC and consequently segregate from other proteins constitutively leaving the secretory pathway, but they are missing CHC22 as an active component to drive coalescence and sorting. Thus domain formation in rodent cells would generate a low level of insulin-responsive vesicles that would be sufficient for initial GLUT4 secretion in response to insulin, followed by recapture and targeting to the GSC. In this case, population of the rodent GSC with GLUT4 is mainly a result of the retrograde recycling pathway. In the case of human cells, CHC22 can actively capture GLUT4 and partners for diversion to the GSC, providing a more vigorous route to GSC formation following biosynthesis, with the GSC then replenished with GLUT4 by the endocytic-retrograde recycling pathway. In both rodent and human cells, CHC17 clathrin performs uptake of GLUT4 from the cell surface (Antonescu et al., 2008; Esk et al., 2010; Robinson et al., 1992; Vassilopoulos et al., 2009), while CHC17 performs retrograde recycling to the GSC in mice (Gillingham et al., 1999; Li and Kandror, 2005) and CHC22 participates in this part of the pathway in humans (Esk et al., 2010) (Fig. 8). This species difference in membrane dynamics of GLUT4 traffic has the effect that human cells cannot form a GSC with only CHC17. However, the presence of CHC22 enhancing biosynthetic GSC formation may have the consequence that humans are able to sequester intracellular GLUT4 more efficiently than species without CHC22, a trait that may also contribute to a tendency to insulin resistance.

MATERIALS AND METHODS

Plasmids

The HA-GLUT4-GFP construct was a gift from Dr Tim McGraw (Lampson et al., 2000). The plasmid encoding human GLUT1 was from OriGene. The haemagglutinin (HA-)tag sequence atcgattatccttatgatgttcctgattatgctgag was inserted at base pair 201 (between amino acids 67 and 68 of the exofacial loop of GLUT1) using the Q5 site-directed mutagenesis kit from New England Biolabs (NEB, USA). HA-GLUT4 and HA-GLUT1 were extracted using AcsI and EcoRI restriction enzymes and Cutsmart buffer and the agarose gel extraction kit from NEB. The inserts were then ligated with the RUSH plasmid containing the ER hook Ii fused to streptavidin (Boncompain et al., 2012; Boncompain and Perez, 2013). The generation of GFP-tagged CHC22 and CHC17 plasmids has been described elsewhere (Esk et al., 2010).

Cell culture

All cell lines were maintained at 37°C in a 5% CO_2 atmosphere. The HeLa cell line stably expressing GLUT4 (HeLa-G4) was generated by transfection of HeLa cells with the plasmid encoding HA-GLUT4-GFP (Dawson et al., 2001; Lampson et al., 2000; Quon et al., 1994). Transfectants were selected in Growth medium supplemented with 700 µg/mL G418 then maintained in growth medium with 500 µg/mL G418. The human skeletal muscle cell line LHCNM2 was described elsewhere (Esk et al., 2010; Vassilopoulos et al., 2009; Zhu et al., 2007). A549 human lung carcinoma cells were obtained from the ATCC. HeLa and A549 cells were grown in Dulbecco's Modified Eagle Medium high glucose supplemented with 10% FBS (Gibco), 50 U/mL penicillin, 50 µg/mL streptomycin (Gibco), 10 mM Hepes (Gibco). LHCNM2 cells were grown in proliferation medium: DMEM MegaCell (Sigma) supplemented with 5% FBS (Gibco), 2 mM L-Glutamine (Sigma), 1% non-essential amino acids (Sigma), 0.05 mM β-mercaptoethanol (Gibco) and 5 ng/mL bFGF (Thermo Fisher). When full confluency was reached, cells were switched to

differentiation medium: DMEM (Sigma) supplemented with 2 mM L-Glutamine (Sigma), 100 IU penicillin and 100 µg/mL streptomycin (Gibco). The human AB1190 human myoblast cell line was immortalized at the Institute of Myology (Paris). These cells were grown in complete Skeletal Muscle Cell Growth Medium (Promocell) supplemented with serum to reach 20% final concentration (V/V). Differentiation of confluent myoblasts was induced by incubating the cells in differentiation medium for 6 to 7 days: DMEM (Gibco), Gentamycin 50 µg/ml (Gibco) + insulin 10 µg/ml (Sigma). All cell lines used were tested negative for mycoplasma infection.

Small RNA interference

Targeting siRNA was produced (Qiagen) to interact with DNA sequences AAGCAATGAGCTGTTTGAAGA for CHC17 (Esk et al., 2010), TCGGGCAAATGTGCCAAGCAA and AACTGGGAGGATCTAGTTAAA for CHC22 (1:1 mixture of siRNAs were used)(Vassilopoulos et al., 2009) and AAGACCGGCAATTGTAGTACT for p115 (Puthenveedu and Linstedt, 2004). Non-targeting control siRNA was the Allstars Negative Control siRNA (Qiagen). siRNA targeting GM130 and scrambled negative control siRNA were purchased from OriGene. For siRNA treatments, cells were seeded (10,000 cells/cm^2) in 6- or 24-well plates in culture medium. The next day, the cells were transfected with siRNAs complexed with JetPrime (PolyPlus). For targeting CHC17, p115 and GM130, 20 nM of siRNA was used per treatment. For targeting CHC22, 20 nM of siRNA was used per treatment, except for Western blot experiments in Figure 6 where 40 nM of siRNA were used. 6 h after siRNA transfection, cells were returned to normal growth conditions and then harvested for analysis or fixed for imaging 72 h later. Silencing was assessed by immunoblotting.

Transfection

For transient DNA transfection, cells were seeded (21,000 cells/cm^2) in 24-well plates in culture medium. The next day, the cells were transfected with plasmidic DNA complexed with JetPrime (PolyPlus) in a 1:2 mixture (DNA/JetPrime). For RUSH experiments, 0.5 mg of DNA was used. 0.25 mg of DNA was used for all other experiments. 6 h after DNA transfection, cells were returned to normal growth conditions and then fixed for imaging 24 h later.

Antibodies and reagents

Primary antibody concentrations ranged from 1-5 µg/mL for immunoblotting and IF assays. Mouse monoclonal anti-CHC17 antibodies (TD.1 (Nathke et al., 1992) and X22 (Brodsky, 1985)), and affinity-purified rabbit polyclonal antibody specific for CHC22 and not CHC17 (Vassilopoulos et al., 2009) were produced in the Brodsky laboratory. Mouse monoclonal anti-p115 antibody (clone 7D1) has been described (Waters et al., 1992). Mouse monoclonal anti-GGA2 was a gift from Dr Juan Bonifacino (US National Institutes of Health, Bethesda, MD, USA). Rabbit polyclonal antibody anti-*L.p.* was a gift from Dr Craig Roy (Yale University, New Haven, CT, USA). Mouse monoclonal antibody anti-*L.p.* was made in the Mukherjee lab. Commercial sources of antibodies were as follows: Rabbit polyclonal anti-CHC17 (Abcam), rabbit polyclonal anti-CHC22 antibody (Proteintech), mouse monoclonal anti-β-COP (clone maD**,** Sigma), rabbit polyclonal anti-IRAP (#3808, Cell Signaling Technology), mouse monoclonal anti-IRAP (clone 3E1, Cell Signaling Technology), rabbit polyclonal anti-phospho AKT Ser473 (#9271, Cell Signaling Technology), rabbit polyclonal anti-phospho-AS160 Thr642 (#4288, Cell Signaling Technology), rabbit polyclonal anti-AS160 (#2447, Cell Signaling Technology), goat polyclonal anti-GLUT4 (C-20, Santa-Cruz Biotechnologies), mouse monoclonal anti-calreticulin (clone FMC75, Stressgen Bioreagents), sheep polyclonal anti-TGN46 (AHP500G, Biorad), goat polyclonal anti-GM130 (P-20, Santa-Cruz Biotechnologies), sheep polyclonal anti-Sec22b (AHP500G, Creative Diagnostics), mouse monoclonal anti-

ERGIC-53 (clone 2B10, OriGene), rabbit polyclonal anti-ERGIC-53 (E1031, Sigma), rabbit monoclonal anti-LMAN1 (clone EPR6979, Abcam), rabbit polyclonal anti-sortilin (ab16640, Abcam), mouse monoclonal anti-STX6 (clone 30/Syntaxin 6, Becton Dickinson), mouse monoclonal anti-β actin (clone AC-15, Sigma), mouse monoclonal anti-HA (clone 16B12, Covance). The commercial anti-CHC22 from Proteintech was confirmed in our laboratory to be specific for CHC22 and not CHC17 (Fig. S1 A). For IF, secondary antibodies coupled to Alexa Fluor 488, Alexa Fluor 555, Alexa Fluor 562 or to Alexa Fluor 647 (Thermo Fisher) were used at 1:500. For Western blotting, antibodies coupled to HRP (Thermo Fisher, Biorad) were used at 1:10,000. Brefeldin A (BFA) was from Sigma.

Legionella pneumophila

WT and *ΔdotA Legionella* strains were gifts from Dr Craig Roy's (Yale University). The parental strain (wild type) was *L.p.* serogroup 1 strain L.p.01, and the variant strain *ΔdotA* were isogenic mutants described previously (Berger et al., 1994; Zuckman et al., 1999). Single colonies of *L.p.* were isolated from charcoal yeast extract plates after growth for 2 days at 37ºC. DsRed-expressing WT *L.p.* were grown on charcoal yeast extract plates containing 500 mM isopropyl+- o-thiogalactopyranoside (IPTG) for 2 days at 37ºC to induce expression of the fluorescent protein.

Infection and analysis of replicative vacuoles

A549 cells were seeded 10^5 cells per 2 cm^2 on coverslips. Cells were infected at a multiplicity of infection (MOI) of 25 with WT or *ΔdotA L.p.* strains. Immediately after adding *L.p.* to the medium, cells were centrifuged at 400 x g for 15 min, then left at 37ºC for an additional 45 min. Cells were then washed 3X with PBS and incubated in growth medium for the indicated time. To analyse replicative vacuoles, cells were transfected with siRNA (20 nM) 72h before infection with WT or *ΔdotA L.p.* at a MOI

of 50 for 1h. siRNA-treated cells were incubated 8h post-infection, then washed 3X with PBS, fixed with 4% paraformaldehyde (PFA) for 30 min and labelled with antibody to detect bacteria for counting the number per replicative vacuole.

Immunofluorescence

Cells grown on 1.5# glass coverslips (Warner Instruments) were washed (PBS, 4°C), fixed (4% PFA, 30 min, 4°C), permeabilized and blocked (PBS 0.5% saponin, 2% bovine serum albumin) for 1 hour at room temperature (RT). Cells were then incubated with primary antibodies (overnight, 4ºC), washed (5X, PBS, 4°C) and incubated with species-specific secondary antibodies coupled to fluorophores (Thermo Fisher). Cells were then washed (5X, PBS, 4°C) and coverslips mounted on microscope slides using Prolong Antifade Diamond kit (Thermo Fisher). Samples were imaged using a Leica TCS SP8 inverted laser scanning confocal microscope equipped with two high sensitivity (HyD) detector channels and one PMT detector channel, a 63X (1.40 NA) HC Plan-Apo CS2 oil-immersion objective and five laser lines. Dyes were sequentially excited at 405 nm (DAPI), 488 nm (GFP, Alexa Fluor 488), 543 nm (Alexa 555), 561 nm (Alexa 568), and 633 nm (Alexa 647). Multicolor images (1024 x 1024 pixels) were saved as TIFF files in Leica LAS X Software (Leica) and input levels were adjusted using ImageJ (US National Institutes of Health, NIH). Labelling detected in individual channels is shown in black and white in figure panels. Merged images are presented in pseudo-color as described in the legends. Image quantification was performed using ImageJ. For each cell, individual marker fluorescence was measured in separate channels, and signals were adjusted to their dynamic ranges. Degree of marker overlap in individual cells was determined by Pearsons' correlation coefficients.

Structured Illumination Microscopy (SIM)

Sample preparation (fixation and staining) steps were identical to confocal microscopy. Sample acquisition was performed on a Zeiss Elyra PS.1 microscope (Axio Observer.Z1 SR, inverted, motorized) through a 100X alpha Plan-Apochromat DIC M27 Elyra lense (oil-immersion, 1.46 NA). Fluorophore excitation was performed with a 50 mW HR diode emitting at 350 nm (BP 420-480/LP 750 filter), and a 200 mW HR diode emitting at 488 nm (BP 495-550/LP 750 filter), a 200 mW HR Diode Pumped Solid State laser emitting at 561 nm (BP 470-620/LP 750 filter) and a 260 mW HR diode emitting at 642 nm (LP 655 filter). Acquisition was performed using a pco.egde sCMOS camera and post-acquisition processing (channel alignment) was performed on the ZEN Black software Version 11.0.2.190.

GLUT4 internalization experiments

The GLUT4 internalization protocol was adapted from previous work (Foley and Klip, 2014). HeLa-GLUT4 cells were seeded on coverslips in 24-well plate and grown to 80% confluency. On the day of the experiment, cells were washed (3X, PBS, 37°C) and serum starved 2 hours. Cell surface HA-GLUT4-GFP was labelled on ice for 30 min with mouse monoclonal anti-HA antibody. After washing (5X, PBS, 4°C), cells were placed in serum-free medium (37°C) for indicated times. Cells were then washed (3X, PBS, 4°C), fixed and processed for immunofluorescence detection of internalised anti-HA antibody.

GLUT4 translocation assay using flow cytometry

HeLa-GLUT4 cells were seeded in 6-well plates and grown to 95% confluency. On the day of experiment, cells were washed (3X, PBS, 37°C), serum-starved (2 hours), then treated with insulin to a final concentration of 170 nM or the same volume of vehicle (water) diluted in serum-free medium for 15 minutes, 37°C. Cells were then placed on ice and rapidly washed (3X, PBS, 4°C) and fixed (PFA 4%, 45 min). After fixation, cells were washed (3X, PBS, RT) then blocked for 1 hour (PBS 2% BSA,

RT) before incubation with monoclonal anti-HA antibody (45 min, RT) to detect surface GLUT4. After incubation, cells were washed (5X, PBS, RT) and incubated with Alexa Fluor 647-anti-mouse Ig (45 min, RT). Cells were then washed (5X, PBS, RT), gently lifted using a cell scraper (Corning), pelleted (200xg, 10 min) and re-suspended (PBS, 2% BSA, 4°C). Data was acquired with Diva acquisition software by LSRII flow cytometer (Becton Dickinson) equipped with violet (405 nm), blue (488 nm) and red (633 nm) lasers. Typically, 10,000 events were acquired and Mean Fluorescence Intensity (MFI) values for surface GLUT4 (Alexa Fluor 647) and total GLUT4 (GFP) were recorded using 660/20 and 530/30 filters, respectively. Post-acquisition analysis was performed using FlowJo software (Treestar) where debris were removed by FSC/SSC light scatter gating then fluorescence histograms were analyzed. The ratio of surface to total MFI was calculated to quantify the extent of GLUT4 translocation.

RUSH assay

HeLa cells were seeded at 30,000 cells/cm^2 on coverslips. The next day, cells were transfected with 0.5 mg of RUSH-HA-GLUT1-SBP-GFP or RUSH-HA-GLUT4-SBP-GFP plasmids for 6h, then switched to fresh medium. The next day, cells were treated with 40 mM biotin for the indicated times. Cells were then quickly placed on ice, washed (3X, PBS, 4°C), fixed (4% PFA, RT) and processed for immunofluorescence.

Alkaline phosphatase secretion assay

HeLa-GLUT4 cells were in 96-well plates and grown to 80% confluency and were transfected the next day with 20 nM targeting or control siRNA. After 48h, cells were transfected with the plasmid encoding secreted alkaline phosphatase. After 24h, fresh medium was added to the culture and 8h later, the media were harvested and the cells lysed. Alkaline phosphatase activity in the harvested medium and cell lysate

was assessed using the Phospha-Light System kit (Applied Biosystems), following the manufacturer's instructions and detected with a luminometer (Varioskan LUX multimode multiplate reader, Thermo Fisher scientific). The alkaline phosphatase secretion index was determined by calculating the ratio of alkaline phosphatase activity detected in the medium (secreted) to total alkaline phosphatase activity in the culture (medium plus cell lysate activity).

Brefeldin A treatment

HeLa-GLUT4 or LHCNM2 myoblasts were grown on coverslips and exposed to BFA (10 ug/mL, 1h, 37°C) or vehicle (DMSO). Cells were then washed (3X, PBS, RT) and processed for immunofluorescence.

Preparation of clathrin-coated vesicles

Clathrin coated vesicles (CCV) preparation was adapted from Keen et al. (Keen et al., 1979). Briefly, pig brains were blended in buffer A (100mM MES, 1mM EDTA, 0.5 mM MgCl2) supplemented with 0.5 mM PMSF. The preparation was centrifuged at 8,000 rpm (JA-17 rotor, Beckman) at 4°C for 30 min, then the supernatant was filtered to remove particles and centrifuged at 40,000 rpm (45 Ti rotor, Beckman) at 4°C for 60 min to pellet the CCVs. A small volume of buffer A supplemented with 0.02 mM PMSF was added to the CCV pellets before homogenization with a potter S homogenizer. A solution of 12.5% Ficoll 12.5% sucrose was added 1:1 to the CCV suspension and gently mixed. The CCV preparation was then centrifuged at 15,000 rpm (JA-17 rotor, Beckman) at 4°C for 40 min. The supernatant was collected, diluted 5-fold in buffer A supplemented with 1 mM phenylmethane sulfonyl fluoride (PMSF) and centrifuged 40,000 rpm (45 Ti rotor, Beckman) for 60 min at 4°C to pellet vesicles. The pellet was resuspended in buffer A for Tris extraction. Finally, the preparation was purified by gel filtration (Superose 6, GE Life Science). CCV were stored at -80ºC in 10 mM Tris–HCl, pH 8.0.

Purification of hub CHC22

Hub CHC22 fragment was produced in BL21(DE3) bacteria (Novagen) by induction with 1 mM IPTG for 24 hr at 12°C. Bacterial pellets were resuspended in LysI (1M NaCl pH8, 20 mM imidazole in PBS) supplemented with 1 mM PMSF, protease inhibitors (1 tab/10 mL, Roche), 40 µg/mL lysozyme, 0.1% b-mercaptoethanol (Sigma). Then LysII (1M NaCl, 0.5M guanidine HCl, 0.4% Triton X100 in PBS) was added at 1:1.25 (LysI:LysII) ratio and samples were spinned at 40,000 rpm for 30 min at 4°C. Supernatant was ran through a Ni+ affinity NTA column, then washed with LysI and eluted with 1M NaCl pH8, 0.5M imidazole in PBS.

Immunoblotting

Protein extracts from cells were quantified by BCA (Pierce), separated by SDS-PAGE (10% acrylamide), transferred to nitrocellulose membrane (0.2 µm, Biorad) and labelled with primary antibodies (1-5 µg/mL), washed and labelled with species-specific horseradish peroxidase-conjugated secondary antibodies (Thermo Fisher). Peroxidase activity was detected using Western Lightning Chemiluminescence Reagent (GE Healthcare). The molecular migration position of transferred proteins was compared to the PageRuler Prestain Protein Ladder 10 to 170 kDa (Thermo Fisher Scientific). Signal quantification was performed using Image J software (NIH).

Immunoprecipitations (IP)

Confluent cells from a 500 cm^2 plate were scrapped off the plate, washed in ice-cold PBS and pelleted (300 g, 8 min, 4ºC). The pellets were resuspended in ice-cold lysis buffer (NaCl 150 mM, HEPES 20 mM, EDTA 1 mM, EGTA 1 mM, Glycerol 10% (V/V), NP-40 0.25% (V/V)) supplemented with protease (1 tab/10mL, Roche) and phosphatase (Na_4VO_3 2 mM) inhibitors. Cell suspensions were mechanically sheared (over 25 passages through a 27G needle), sonicated and spun down (500 g for 10

min, 4ºC) to remove nuclei. Specific anti-CHC22 (proteintech) and CHC17 (X-22) antibodies were incubated at 10 ug/mL with 7 mg of pre-cleared post-nuclear supernatants (overnight, 4ºC). The samples were then incubated with washed protein G sepharose (PGS, 25 uL, GE Healthcare) for 1h (4ºC) before three consecutive washing steps in lysis buffer. Pelleted PGS were resuspended in 30 uL of 1X sample buffer and subjected to SDS PAGE and immunoblotting. HRP-conjugated Trueblot secondary antibodies (Rockland) were used for immunoblotting IP experiments.

Statistical analyses

All calculations and graphs were performed with Microsoft Excel and GraphPad Prism softwares. P-values were calculated using unpaired two-tailed Student's t-tests or two-way ANOVA followed by Tukey or Sidak's multiple comparisons test. Detailed statistical information including statistical test used, number of independent experiments, *p* values, definition of error bars is listed in individual figure legends. All experiments were performed at least three times, except for the immunoblots shown in Figs. 1 C and 7 A and the infection experiment shown in Fig. S4 C, which were performed twice. Immunofluorescence staining showed in Figs. 1 D and S3 were performed once.

Figure Legends

Figure 1: HeLa-GLUT4 cells have a functional GLUT4 trafficking pathway that requires CHC22.

(A) Representative images of GLUT4 (exofacial hemagglutinin (HA)-tag, internal GFP tag) in HeLa-GLUT4 cells before (basal) or after insulin treatment. GLUT4 at the plasma membrane was detected by immunofluorescence (IF) after surface labeling with anti-HA monoclonal antibody (red). Total GLUT4 (green) was detected by GFP tag. Arrows show the GLUT4 storage compartment. Arrowheads point to peripheral vesicles. Scale bars: 7.5 μm. (B) Left panel – Representative FACS histogram of surface GLUT4 fluorescence intensities (signal from anti-HA labeling) before (basal) and after insulin treatment. Right panel – quantification of surface:total GLUT4 (HA:GFP mean fluorescence intensity signals). Data expressed as mean ± SEM, N=3, 10,000 cells acquired per experiment. Two-tailed unpaired Student's t-test with equal variances, **$p<0.01$. (C) Representative immunoblot for phosphorylated AKT (p-AKT), phosphorylated AS160 (p-AS160), total AS160 and β-actin in HeLa-GLUT4 cells before (basal) and after insulin treatment. The migration position of molecular weight (MW) markers is indicated at the left in kilodaltons (kDa). (D) Left panel - representative Structured Illumination Microscopy (SIM) image of a HeLa-GLUT4 cell stained for syntaxin-6 (STX6, red). Total GLUT4 (green) was detected by GFP tag. The gray circle delineates the nucleus (N) and the white square delineates the magnified area displayed in the right panel image. Scale bar: 10 μm. Right panel - the white dashed line in the magnified area spans the segment over which fluorescence intensities for GLUT4 and STX6 are plotted below, in green and red, respectively. Arrowheads indicate areas of overlap. (E) Representative IF staining for internalized surface-labeled GLUT4 (HA-tag, blue) and syntaxin 6 (STX-6, red) for HeLa-GLUT4 cells at 0, 10 or 30 minutes after insulin treatment. Total GLUT4 is detected by GFP tag (green). Scale bars: 7.5 μm. (F) Pearson's overlap quantification for labeling of STX-6 and HA-tag (Data expressed as mean ± SEM,

N=3, 14-19 cells per experiment). One-way analysis of variance (ANOVA) followed by Bonferroni's multiple comparison post-hoc test ****p<0.0001. (G) Representative IF staining for CHC17 (red) and CHC22 (blue) in HeLa-GLUT4 cells transfected with control siRNA (non-targeting) or siRNA targeting CHC17 (siCHC17) or CHC22 (siCHC22), with GLUT4 detected by GFP tag (green). Arrows point to a CHC22-depleted cell. Scale bars: 10 µm for siControl and siCHC17 and 7.5 µm for siCHC22. (H) Representative FACS histograms of surface GLUT4 fluorescence intensity (signal from anti-HA labeling) in HeLa-GLUT4 cells transfected with control siRNA or siRNA targeting CHC22 (siCHC22) before (basal; red) or after treatment with insulin (insulin; blue). Histograms are extracted from the experiment quantified in Fig. 7 F. Merged images in (A), (D), (E), (G) show red/green overlap in yellow, red/blue overlap in magenta, green/blue overlap in turquoise, and red/green/blue overlap in white.

Figure 2: Newly synthesized GLUT4 is delayed in the early secretory pathway compared to GLUT1.

(A, C, E, G, I) Representative immunofluorescence staining for GLUT1-SBP-GFP or GLUT4-SBP-GFP (green), CHC22 (red) and (A) calnexin (CNX), (C) ERGIC-53, (E) p115, (G) GM130 or (I) TGN46 (blue) in HeLa cells transfected with RUSH-HA-GLUT1-SBP-GFP or RUSH-HA-GLUT4-SBP-GFP. The type II ER resident protein Ii fused to streptavidin was used as an ER hook. Trafficking of GLUT4 and GLUT1 was tracked at 0, 15, 30 and 60 minutes after release from the endoplasmic reticulum (ER) by biotin. Arrows point to GLUT1 detected at the plasma membrane and arrowheads point to GLUT1-positive endosomal structures. Merged images show red/green overlap in yellow, red/blue overlap in magenta, green/blue overlap in turquoise, and red/green/blue overlap in white. Scale bars: 10 µm. (B, D, F, H, J, K) Pearson's overlap between GFP (GLUT1 or GLUT4) and calnexin (CNX), ERGIC-53, p115, GM130, TGN46 or CHC22 at different time points post-ER release. Data

expressed as mean ± SEM, N=3-4, 10-46 cells per experiment. One-way analysis of variance (ANOVA) followed by Sidak's multiple comparison post-hoc test *p<0.05, **p<0.01, ****p<0.0001 to test differences between GLUT1-GFP and GLUT4-GFP overlap with markers at each time points.

Figure 3: CHC22 is localized at the ER-to-Golgi Intermediate Compartment in HeLa GLUT4 and human myotubes.

(A) Pearson's overlap between CHC22 and GLUT4, calreticulin (endoplasmic reticulum), ERGIC markers p115 and ERGIC-53, cis-Golgi marker GM130 or trans-Golgi marker TGN46 in HeLa-GLUT4 from images taken by confocal microscopy (corresponding representative immunofluorescence staining in Fig. S1). Data expressed as mean ± SEM, N=3, 4-10 cells across 3 independent samples. (B) Representative Structured Illumination Microscopy of a HeLa-GLUT4 cell and human skeletal muscle cell AB1190 (hSKMC) stained for CHC22 (red) and p115 (blue). GLUT4 (green) was detected by GFP tag. The gray circles delineate the nuclei (N). Muscle cell staining with each antibody is shown in black on white below the color images. Scale bars: 10 µm. (C, D, E, F) Representative Structured Illumination Microscopy of the perinuclear region of HeLa-GLUT4 cells and hSKMC (AB1190) stained for CHC22 (red) and p115, ERGIC-53, GM130 or TGN46 (blue). GLUT4 (green) was detected by GFP tag. The solid gray lines delineate the nuclear border (N). The dashed white lines span the segment over which fluorescence intensities for GLUT4 (green), CHC22 (red) and p115, ERGIC-53, GM130 or TGN46 (blue) were plotted. Arrowheads indicate areas of peak overlap. Scale bars: 1 µm. Merged images in (B, C, D, E, F) show red/green overlap in yellow, red/blue overlap in magenta, green/blue overlap in turquoise, and red/green/blue overlap in white.

Figure 4: CHC22 participates in membrane trafficking from the ERGIC.

(A) Representative images of *Legionella pneumophila* (*L.p.*)-infected A549 cells transiently transfected with GFP-tagged CHC22 or CHC17 (green). One hour after infection with either wild type (WT) or mutant *Δ dotA L.p.* (MOI=50), bacteria were detected by immunofluorescence (IF, red). Arrows point to *L.p.* and boxed inserts (upper right or left) show *L.p.* region at 5X magnification. Scale bars: 10 µm for cells expressing CHC22-GFP and 7.5 µm for cells expressing CHC17-GFP. (B) Quantification of the proportion of *L.p.* vacuoles positive for CHC22 or CHC17. Data expressed as mean ± SEM, N=3, 4 to 35 vacuoles counted per experiment performed as represented in (A). One-way analysis of variance (ANOVA) followed by Bonferroni's multiple comparison post-hoc test ***p<0.001. (C) Representative images of A549 cells infected with WT *L.p.* (MOI=50) immunolabeled for endogenous CHC22 or CHC17 (red) and *L.p.* (green) by IF. Arrows point to *L.p.*, dashed lines delineate cell borders. Scale bar: 5 µm. (D) Quantification of the proportion of replicative vacuoles (8 hours post-infection) containing 1, 2 to 4, or more than 4 WT or *Δ dotA L.p.* after treatment with siRNA targeting CHC22 or CHC17 or control siRNA. Data expressed as mean ± SEM, N=3, over 140 vacuoles counted per experiment. One-way ANOVA followed by Bonferroni's multiple comparison post-hoc test was performed to compare the number of cells with a vacuole containing more than 4 bacteria. ****p<0.0001 versus siControl-transfected cells infected with WT *L.p.*. ++++p<0.0001 versus siControl-transfected cells infected with *Δ dotA L.p.* Merged images in (A) and (C) show red/green overlap in yellow.

Figure 5: The *L.p.* vacuole acquires proteins involved in GSC formation.
(A) Quantification of the proportion of *L.p.* vacuoles positive for GLUT4-GFP, p115, GGA2, sortilin, IRAP or Rab1 1h after infection with WT or *Δ dotA L.p.* in HeLa cells transiently expressing FcγRII (needed for *L.p.* infection) (Arasaki and Roy, 2010). Data expressed as mean ± SEM, N=3, 4 to 50 vacuoles counted per experiment.

Two-tailed unpaired Student's t-test with equal variances: *p<0.05, **p<0.01, ***p<0.001. (B-F) Representative immunofluorescence of HeLa cells one hour after infection with either wild type (WT) or mutant *Δ dotA L.p.* (MOI=50) stained for *L.p.* (red) and p115, IRAP, GGA2, sortilin or Rab1 (green). Hoechst stains the nuclei (blue). Arrows point to *L.p.*-containing vacuoles, Scale bars: 10 µm. Merged images show red/green overlap in yellow.

Figure 6: **CHC22 interacts with p115 and each influences stability of different partners for GLUT4 membrane traffic.**

(A, B) Representative immunoblots of CHC22 or CHC17 immunoprecipitations from HeLa cell (A) and CHC22 immunoprecipitation from hSKMC (AB1190) (B) analyzed for CHC22, CHC17 or p115. (C, E) Representative immunoblots of HeLa-GLUT4 cells transfected with siRNA targeting CHC22, CHC17 or p115 or with control siRNA (40 nM for 72h) showing levels of CHC22, GLUT4, GGA2, CHC17, p115, sortilin and β-actin. (D) Representative immunoblots of HeLa-GLUT4 cells transfected with siRNA targeting CHC22, CHC17 or p115 or with control siRNA showing levels of IRAP and β-actin. The position of molecular weight (MW) markers is indicated in kilodaltons (kDa) in (A-E). (F-H) Quantification of immunoblot signals as shown in (C-E). Blot signals were normalized to β-actin for each experiment and the fold change (negative values indicate decrease and positive values indicate increase) relative to the normalized signal in control siRNA-treated cell lysates is plotted. Data expressed as mean ± SEM, N=7-8. Two-tailed unpaired Student's t-test, with Welch's correction where variances were unequal: *p<0.05; ***p<0.001, ****p<0.0001.

Figure 7: Membrane traffic to the human GSC requires CHC22 and p115, but not GM130.

(a) Immunoblotting for CHC22, CHC17, p115, GM130 and β-actin after transfection of HeLa-G4 cells with siRNA targeting CHC17, CHC22, p115, GM130 or with control (non-targeting) siRNA. The position of molecular weight (MW) markers is indicated in kilodaltons (kDa). (B) Representative immunofluorescence (IF) staining for CHC22 (red) and p115 (blue) in HeLa-GLUT4 cells after siRNA transfection as in (A), with GLUT4 detected by GFP tag (green). N, nuclei. Arrow points to CHC22-depleted cell. Scale bars: 10 µm. (C) Representative IF staining for GM130 (yellow), p115 (red) and CHC22 (blue) in HeLa-GLUT4 cells after treatment with siRNA targeting GM130 or with control siRNA, with GLUT4 detected by GFP tag (green). Scale bars: 25 µm. (D) FACS quantification of surface:total GLUT4 in HeLa-G4 cells treated with siRNA targeting CHC22, CHC17, p115 or GM130 or with control siRNA with (+) or without (-) exposure to insulin. Data expressed as mean ± SEM, N=9, 10,000 cells acquired per experiment. One-way ANOVA followed by Bonferroni's multiple comparison post-hoc test **$p<0.01$, ***$p<0.001$, ****$p<0.0001$ versus untreated (-).

Figure 8: Model for human GSC biogenesis from the secretory and endocytic pathways.

Newly synthesized GLUT4, IRAP and sortilin traffic from the endoplasmic reticulum (depicted in box A) to the ER-to-Golgi Intermediate Compartment (ERGIC). At the ERGIC, a stable complex forms between IRAP and p115 that promotes binding of GLUT4. Sortilin interacts with both IRAP and GLUT4 recruiting GGA2 and CHC22 to a protein sorting domain (depicted in box B). Formation of the CHC22 clathrin coat at the ERGIC then facilitates sorting of GLUT4, IRAP and sortilin to the GSC. Vesicles containing GLUT4 and IRAP are generated at the GSC for translocation to the plasma membrane in response to insulin. From the plasma membrane, GLUT4 undergoes CHC17 clathrin-dependent endocytosis, and is recycled back to the GSC via the retrograde pathway from late endosomes to the TGN by CHC22.

SUPPLEMENTARY INFORMATION

Figure S1: Immunofluorescence localization of CHC22 at the ER-to-Golgi Intermediate Compartment in HeLa GLUT4 cells and in human skeletal muscle cells.

(A) CHC17 (X22 antibody) or CHC22 (CLTCL1 antibody) immunoblots (IB) of clathrin coated vesicles (CCV) purified from pig brain containing only CHC17 or of cell lysate from bacteria expressing low levels of the hub fragment (residues 1074-1640) of CHC22 (hub 22). The position of molecular weight (MW) markers is indicated in kilodaltons (kDa). Ponceau staining for protein is shown on the right (Pro). (B) Representative confocal microscopy immunofluorescence (IF) imaging of CHC22 (red or blue), p115 (red or blue) and GLUT4 (green) in HeLa-GLUT4 cells (top panel) or LHCNM2 myotubes (bottom panel). (C) Representative IF staining for CHC22 (blue), ERGIC-53 (red) and GLUT4 (green) in HeLa-GLUT4 cells (top panel) or LHCNM2 myotubes (bottom panel). Scale bars: 5 µm for HeLa GLUT4 cells and 7.5 µm for hSKMC in (B) and (C). (D) Representative IF staining for CHC22 (blue), GM130 or TGN46 (red) and GLUT4 (GFP, green) in HeLa-GLUT4 cells. Scale bars: 5 µm. (E) Representative IF staining for CHC22 (blue), GM130 or TGN46 (green) and p115 (red) in LHCNM2 myotubes. Scale bars: 7.5 µm. (F) Representative IF staining for CHC22 (blue), calreticulin (red) and GLUT4 (green) in HeLa-GLUT4 cells. Scale bars: 5 µm. (G) Representative IF staining for CHC22 (red), calnexin (CNX, blue) and GLUT4 (green) in hSKMC (AB1190). Scale bars: 10 µm. (H) Representative Structured Illumination Microscopy (SIM) of a HeLa-GLUT4 cell (top panel) and human skeletal muscle cell (AB1190) (hSKMC, bottom panel) stained for CHC22 (red) and TGN46 (blue). GLUT4 (green) was detected by GFP tag. Scale bar: 10 µm. Merged images in (B-H) show red/green overlap in yellow, red/blue overlap in magenta, green/blue overlap in turquoise, and red/green/blue overlap in white. (I) Representative fluorescence intensity plots for GLUT4 (green), CHC22

(red) and p115, ERGIC-53, GM130 or TGN46 (blue) generated from SIM images of the perinuclear region of HeLa-GLUT4 cells.

Figure S2: Surface GLUT4 is recycled to the GSC in proximity to the ERGIC.

(A) Representative immunofluorescence (IF) staining for internalized surface-labeled GLUT4 (HA-tag, blue) and CHC22 (red) for HeLa-GLUT4 cells at 0, 10 or 30 minutes after insulin treatment. Total GLUT4 is detected by GFP tag (green). Scale bars: 5 µm. (B) Pearson's overlap for labeling of CHC22 and HA-tag (data expressed as mean ± SEM, N=3**,** 8-40 cells per experiment). One-way analysis of variance (ANOVA) followed by Bonferroni's multiple comparison post-hoc test *$p<0.05$, ****$p<0.0001$. (C) Representative immunofluorescence (IF) staining for internalized surface-labeled GLUT4 (HA-tag, blue) and ERGIC-53 (red) for HeLa-GLUT4 cells at 0, 10 or 30 minutes after insulin treatment. Total GLUT4 is detected by GFP tag (green). Scale bars: 10 µm. (D) Pearson's overlap for labeling of ERGIC-53 and HA-tag (data expressed as mean ± SEM, N=3**,** 14-22 cells per experiment). One-way analysis of variance (ANOVA) followed by Bonferroni's multiple comparison post-hoc test ****$p<0.0001$. Merged images show red/green overlap in yellow, red/blue overlap in magenta, green/blue overlap in turquoise, and red/green/blue overlap in white.

Figure S3: CHC22 re-distributes with p115 following Brefeldin A treatment.

Representative immunofluorescence (IF) staining for CHC22 (blue) and p115 (red) in (A) HeLa-GLUT4 cells or (B) LHCNM2 myotubes treated or not with Brefeldin A (BFA). GLUT4 (green) was detected by GFP tag in HeLa-G4 cells and by IF of endogenous protein in LHCNM2 cells. Scale bars: 5 and 25 µm for (A) and (B), respectively. Merged images show red/green overlap in yellow, red/blue overlap in magenta, green/blue overlap in turquoise, and red/green/blue overlap in white.

Figure S4: GLUT4 is not recruited to *Legionella pneumophila*'s replicative vacuole.

(A) Representative immunofluorescence images of single A549 cells from cultures treated with siRNA targeting CHC22 or with control (non-targeting) siRNA and labeled for Sec22b (red) and CHC22 (green), 1h post-infection with wild-type *L.p.* (MOI=50). Arrows point to *L.p.* detected with DAPI. Boxed inserts show *L.p.* region at 5X and 2X magnification for siControl and siCHC22, respectively. Scale bar: 5 µm referring to main images. (B) Quantification of the proportion of *L.p.* vacuoles staining positive for Sec22b. Data expressed as mean ± SEM, N=4, 10 to 20 vacuoles counted per experiment as represented in (A). Two-tailed unpaired Student's t-test with equal variances ***$p<0.001$. (C) Representative images of A549 cells transiently transfected with HA-GLUT4-GFP (green), infected with wild type *L.p.* expressing mono-DsRed protein (*L.p.*-DsRed, MOI=50, red) and labeled 1 hour post-infection with antibodies against endogenous CHC17 (upper panel) or CHC22 (lower panel) (blue). Scale bars: 5 µm. (D) Representative immunofluorescence of HeLa cells transiently expressing FcγRII one hour after infection with either wild type (WT) or mutant *Δdot*A *L.p.* (MOI=50) stained for *L.p.* (red) and Sec16a (green). Hoechst stains the nuclei (blue). Arrows point to *L.p.*, Scale bar: 10 µm. (E) Quantification of the proportion of vacuoles staining positive for Sec16a. Data expressed as mean ± SEM, N=3, 50 vacuoles counted per experiment as represented in (D). Merged images in (A, C and D) show red/green overlap in yellow, red/blue overlap in magenta, green/blue overlap in turquoise, and red/green/blue overlap in white. Merged images in (D) show red/green overlap in yellow.

Figure S5: CHC22 localization with GSC marker IRAP and GM130 depletion does not affect the secretion of alkaline phosphatase in HeLa cells.

(A) Left panel - representative Structured Illumination Microscopy of a HeLa-GLUT4 cell stained for CHC22 (red) and IRAP (blue). Total GLUT4 (green) was detected by GFP tag. The gray oval delineates the nucleus (N) and the white square delineates the magnified area displayed in the right panel image. Scale bar: 10 μm. Right panel - the white dashed line in the magnified area spans the segment over which fluorescence intensities for GLUT4, CHC22 and IRAP are plotted below, in green, red and blue, respectively. Arrowheads indicate area of overlap between CHC22 and IRAP. (B) Quantification of alkaline phosphatase secretion index for HeLa-G4 cells treated with siRNA targeting CHC22, CHC17, p115 or GM130 or with control siRNA. The alkaline phosphatase secretion index is the ratio of secreted enzyme activity (culture medium) to total cellular activity (secreted plus cell lysate). Data expressed as mean ± SEM, N=13-19 independent samples across 2 independent assays. One-way analysis of variance (ANOVA) followed by Bonferroni's multiple comparison post-hoc test **$p<0.01$ versus siControl.

References

Alvarez, C., R. Garcia-Mata, H.P. Hauri, and E. Sztul. 2001. The p115-interactive proteins GM130 and giantin participate in endoplasmic reticulum-Golgi traffic. *J Biol Chem*. 276:2693-2700.

Antonescu, C.N., M. Diaz, G. Femia, J.V. Planas, and A. Klip. 2008. Clathrin-dependent and independent endocytosis of glucose transporter 4 (GLUT4) in myoblasts: regulation by mitochondrial uncoupling. *Traffic*. 9:1173-1190.

Arasaki, K., and C.R. Roy. 2010. Legionella pneumophila promotes functional interactions between plasma membrane syntaxins and Sec22b. *Traffic*. 11:587-600.

Berger, K.H., J.J. Merriam, and R.R. Isberg. 1994. Altered intracellular targeting properties associated with mutations in the Legionella pneumophila dotA gene. *Mol Microbiol*. 14:809-822.

Bogan, J.S. 2012. Regulation of glucose transporter translocation in health and diabetes. *Annu Rev Biochem*. 81:507-532.

Boncompain, G., S. Divoux, N. Gareil, H. de Forges, A. Lescure, L. Latreche, V. Mercanti, F. Jollivet, G. Raposo, and F. Perez. 2012. Synchronization of secretory protein traffic in populations of cells. *Nat Methods*. 9:493-498.

Boncompain, G., and F. Perez. 2013. Fluorescence-based analysis of trafficking in mammalian cells. *Methods Cell Biol*. 118:179-194.

Brodsky, F.M. 1985. Clathrin structure characterized with monoclonal antibodies. I. Analysis of multiple antigenic sites. *J Cell Biol*. 101:2047-2054.

Brodsky, F.M. 2012. Diversity of clathrin function: new tricks for an old protein. *Annu Rev Cell Dev Biol*. 28:309-336.

Bruno, J., A. Brumfield, N. Chaudhary, D. Iaea, and T.E. McGraw. 2016. SEC16A is a RAB10 effector required for insulin-stimulated GLUT4 trafficking in adipocytes. *J Cell Biol*. 214:61-76.

Bryant, N.J., R. Govers, and D.E. James. 2002. Regulated transport of the glucose transporter GLUT4. *Nat Rev Mol Cell Biol*. 3:267-277.

Dannhauser, P.N., S.M. Camus, K. Sakamoto, L.A. Sadacca, J.A. Torres, M.D. Camus, K. Briant, S. Vassilopoulos, A. Rothnie, C.J. Smith, and F.M. Brodsky. 2017. CHC22 and CHC17 clathrins have distinct biochemical properties and display differential regulation and function. *J Biol Chem*. 292:20834-20844.

Dawson, K., A. Aviles-Hernandez, S.W. Cushman, and D. Malide. 2001. Insulin-regulated trafficking of dual-labeled glucose transporter 4 in primary rat adipose cells. *Biochem Biophys Res Commun*. 287:445-454.

Derre, I., and R.R. Isberg. 2004. Legionella pneumophila replication vacuole formation involves rapid recruitment of proteins of the early secretory system. *Infect Immun*. 72:3048-3053.

Dobson, S.P., C. Livingstone, G.W. Gould, and J.M. Tavare. 1996. Dynamics of insulin-stimulated translocation of GLUT4 in single living cells visualised using green fluorescent protein. *FEBS Lett*. 393:179-184.

Esk, C., C.Y. Chen, L. Johannes, and F.M. Brodsky. 2010. The clathrin heavy chain isoform CHC22 functions in a novel endosomal sorting step. *J Cell Biol*. 188:131-144.

Fazakerley, D.J., S.P. Lawrence, V.A. Lizunov, S.W. Cushman, and G.D. Holman. 2009. A common trafficking route for GLUT4 in cardiomyocytes in response to insulin, contraction and energy-status signalling. *J Cell Sci*. 122:727-734.

Fisher, P., and D. Ungar. 2016. Bridging the Gap between Glycosylation and Vesicle Traffic. *Front Cell Dev Biol*. 4:15.

Foley, K.P., and A. Klip. 2014. Dynamic GLUT4 sorting through a syntaxin-6 compartment in muscle cells is derailed by insulin resistance-causing ceramide. *Biol Open*. 3:314-325.

Garvey, W.T., L. Maianu, J.H. Zhu, G. Brechtel-Hook, P. Wallace, and A.D. Baron. 1998. Evidence for defects in the trafficking and translocation of GLUT4 glucose transporters in skeletal muscle as a cause of human insulin resistance. *J Clin Invest*. 101:2377-2386.

Ge, L., D. Melville, M. Zhang, and R. Schekman. 2013. The ER-Golgi intermediate compartment is a key membrane source for the LC3 lipidation step of autophagosome biogenesis. *Elife*. 2:e00947.

Ge, L., and R. Schekman. 2014. The ER-Golgi intermediate compartment feeds the phagophore membrane. *Autophagy*. 10:170-172.

Gillingham, A.K., F. Koumanov, P.R. Pryor, B.J. Reaves, and G.D. Holman. 1999. Association of AP1 adaptor complexes with GLUT4 vesicles. *J Cell Sci*. 112 (Pt 24):4793-4800.

Haga, Y., K. Ishii, and T. Suzuki. 2011. N-glycosylation is critical for the stability and intracellular trafficking of glucose transporter GLUT4. *J Biol Chem*. 286:31320-31327.

Hood, F.E., and S.J. Royle. 2009. Functional equivalence of the clathrin heavy chains CHC17 and CHC22 in endocytosis and mitosis. *J Cell Sci*. 122:2185-2190.

Hosaka, T., C.C. Brooks, E. Presman, S.K. Kim, Z. Zhang, M. Breen, D.N. Gross, E. Sztul, and P.F. Pilch. 2005. p115 Interacts with the GLUT4 vesicle protein, IRAP, and plays a critical role in insulin-stimulated GLUT4 translocation. *Mol Biol Cell*. 16:2882-2890.

Hoshino, S., K. Sakamoto, S. Vassilopoulos, S.M. Camus, C.A. Griffin, C. Esk, J.A. Torres, N. Ohkoshi, A. Ishii, A. Tamaoka, B.H. Funke, R. Kucherlapati, M. Margeta, T.A. Rando, and F.M. Brodsky. 2013. The CHC22 clathrin-GLUT4 transport pathway contributes to skeletal muscle regeneration. *PLoS One*. 8:e77787.

Hresko, R.C., H. Murata, B.A. Marshall, and M. Mueckler. 1994. Discrete structural domains determine differential endoplasmic reticulum to Golgi transit times for glucose transporter isoforms. *J Biol Chem*. 269:32110-32119.

Huang, G., D. Buckler-Pena, T. Nauta, M. Singh, A. Asmar, J. Shi, J.Y. Kim, and K.V. Kandror. 2013. Insulin responsiveness of glucose transporter 4 in 3T3-L1 cells depends on the presence of sortilin. *Mol Biol Cell*. 24:3115-3122.

Hudson, A.W., M. Ruiz, and M.J. Birnbaum. 1992. Isoform-specific subcellular targeting of glucose transporters in mouse fibroblasts. *J Cell Biol*. 116:785-797.

Jaldin-Fincati, J.R., M. Pavarotti, S. Frendo-Cumbo, P.J. Bilan, and A. Klip. 2017. Update on GLUT4 Vesicle Traffic: A Cornerstone of Insulin Action. *Trends Endocrinol Metab*. 28:597-611.

Johannes, L., and V. Popoff. 2008. Tracing the retrograde route in protein trafficking. *Cell*. 135:1175-1187.

Kagan, J.C., and C.R. Roy. 2002. Legionella phagosomes intercept vesicular traffic from endoplasmic reticulum exit sites. *Nat Cell Biol*. 4:945-954.

Kagan, J.C., M.P. Stein, M. Pypaert, and C.R. Roy. 2004. Legionella subvert the functions of Rab1 and Sec22b to create a replicative organelle. *J Exp Med*. 199:1201-1211.

Kandror, K.V., and P.F. Pilch. 2011. The sugar is sIRVed: sorting Glut4 and its fellow travelers. *Traffic*. 12:665-671.

Keen, J.H., M.C. Willingham, and I.H. Pastan. 1979. Clathrin-coated vesicles: isolation, dissociation and factor-dependent reassociation of clathrin baskets. *Cell*. 16:303-312.

Kondylis, V., and C. Rabouille. 2003. A novel role for dp115 in the organization of tER sites in Drosophila. *J Cell Biol*. 162:185-198.

Lahtinen, U., U. Hellman, C. Wernstedt, J. Saraste, and R.F. Pettersson. 1996. Molecular cloning and expression of a 58-kDa cis-Golgi and intermediate compartment protein. *J Biol Chem*. 271:4031-4037.

Lamb, C.A., R.K. McCann, J. Stockli, D.E. James, and N.J. Bryant. 2010. Insulin-regulated trafficking of GLUT4 requires ubiquitination. *Traffic*. 11:1445-1454.

Lampson, M.A., A. Racz, S.W. Cushman, and T.E. McGraw. 2000. Demonstration of insulin-responsive trafficking of GLUT4 and vpTR in fibroblasts. *J Cell Sci*. 113 (Pt 22):4065-4076.

Larance, M., G. Ramm, J. Stockli, E.M. van Dam, S. Winata, V. Wasinger, F. Simpson, M. Graham, J.R. Junutula, M. Guilhaus, and D.E. James. 2005. Characterization of the role of the Rab GTPase-activating protein AS160 in insulin-regulated GLUT4 trafficking. *J Biol Chem*. 280:37803-37813.

Leto, D., and A.R. Saltiel. 2012. Regulation of glucose transport by insulin: traffic control of GLUT4. *Nat Rev Mol Cell Biol*. 13:383-396.

Li, L.V., and K.V. Kandror. 2005. Golgi-localized, gamma-ear-containing, Arf-binding protein adaptors mediate insulin-responsive trafficking of glucose transporter 4 in 3T3-L1 adipocytes. *Mol Endocrinol*. 19:2145-2153.

Liu, S.H., M.C. Towler, E. Chen, C.Y. Chen, W. Song, G. Apodaca, and F.M. Brodsky. 2001. A novel clathrin homolog that co-distributes with cytoskeletal components functions in the trans-Golgi network. *EMBO J*. 20:272-284.

Machner, M.P., and R.R. Isberg. 2006. Targeting of host Rab GTPase function by the intravacuolar pathogen Legionella pneumophila. *Dev Cell*. 11:47-56.

Maianu, L., S.R. Keller, and W.T. Garvey. 2001. Adipocytes exhibit abnormal subcellular distribution and translocation of vesicles containing glucose transporter 4 and insulin-regulated aminopeptidase in type 2 diabetes mellitus: implications regarding defects in vesicle trafficking. *J Clin Endocrinol Metab*. 86:5450-5456.

Martin, O.J., A. Lee, and T.E. McGraw. 2006. GLUT4 distribution between the plasma membrane and the intracellular compartments is maintained by an insulin-modulated bipartite dynamic mechanism. *J Biol Chem*. 281:484-490.

Martin, S., G. Ramm, C.T. Lyttle, T. Meerloo, W. Stoorvogel, and D.E. James. 2000. Biogenesis of insulin-responsive GLUT4 vesicles is independent of brefeldin A-sensitive trafficking. *Traffic*. 1:652-660.

Mukherjee, S., X. Liu, K. Arasaki, J. McDonough, J.E. Galan, and C.R. Roy. 2011. Modulation of Rab GTPase function by a protein phosphocholine transferase. *Nature*. 477:103-106.

Nahorski, M.S., L. Al-Gazali, J. Hertecant, D.J. Owen, G.H. Borner, Y.C. Chen, C.L. Benn, O.P. Carvalho, S.S. Shaikh, A. Phelan, M.S. Robinson, S.J. Royle, and C.G. Woods. 2015. A novel disorder reveals clathrin heavy chain-22 is essential for human pain and touch development. *Brain*. 138:2147-2160.

Nahorski, M.S., G.H.H. Borner, S.S. Shaikh, A.K. Davies, L. Al-Gazali, R. Antrobus, and C.G. Woods. 2018. Clathrin heavy chain 22 contributes to the control of neuropeptide degradation and secretion during neuronal development. *Sci Rep*. 8:2340.

Nathke, I.S., J. Heuser, A. Lupas, J. Stock, C.W. Turck, and F.M. Brodsky. 1992. Folding and trimerization of clathrin subunits at the triskelion hub. *Cell*. 68:899-910.

Nielsen, M.S., P. Madsen, E.I. Christensen, A. Nykjaer, J. Gliemann, D. Kasper, R. Pohlmann, and C.M. Petersen. 2001. The sortilin cytoplasmic tail conveys Golgi-endosome transport and binds the VHS domain of the GGA2 sorting protein. *EMBO J*. 20:2180-2190.

Niu, T.K., A.C. Pfeifer, J. Lippincott-Schwartz, and C.L. Jackson. 2005. Dynamics of GBF1, a Brefeldin A-sensitive Arf1 exchange factor at the Golgi. *Mol Biol Cell*. 16:1213-1222.

Orme, C.M., and J.S. Bogan. 2012. The ubiquitin regulatory X (UBX) domain-containing protein TUG regulates the p97 ATPase and resides at the endoplasmic reticulum-golgi intermediate compartment. *J Biol Chem*. 287:6679-6692.

Perera, H.K., M. Clarke, N.J. Morris, W. Hong, L.H. Chamberlain, and G.W. Gould. 2003. Syntaxin 6 regulates Glut4 trafficking in 3T3-L1 adipocytes. *Mol Biol Cell*. 14:2946-2958.

Piao, H., J. Kim, S.H. Noh, H.S. Kweon, J.Y. Kim, and M.G. Lee. 2017. Sec16A is critical for both conventional and unconventional secretion of CFTR. *Sci Rep*. 7:39887.

Puertollano, R., P.A. Randazzo, J.F. Presley, L.M. Hartnell, and J.S. Bonifacino. 2001. The GGAs promote ARF-dependent recruitment of clathrin to the TGN. *Cell*. 105:93-102.

Puthenveedu, M.A., and A.D. Linstedt. 2004. Gene replacement reveals that p115/SNARE interactions are essential for Golgi biogenesis. *Proc Natl Acad Sci U S A*. 101:1253-1256.

Quon, M.J., M. Guerre-Millo, M.J. Zarnowski, A.J. Butte, M. Em, S.W. Cushman, and S.I. Taylor. 1994. Tyrosine kinase-deficient mutant human insulin receptors (Met1153-->Ile) overexpressed in transfected rat adipose cells fail to mediate translocation of epitope-tagged GLUT4. *Proc Natl Acad Sci U S A*. 91:5587-5591.

Robinson, L.J., S. Pang, D.S. Harris, J. Heuser, and D.E. James. 1992. Translocation of the glucose transporter (GLUT4) to the cell surface in permeabilized 3T3-L1 adipocytes: effects of ATP insulin, and GTP gamma S and localization of GLUT4 to clathrin lattices. *J Cell Biol*. 117:1181-1196.

Sano, H., L. Eguez, M.N. Teruel, M. Fukuda, T.D. Chuang, J.A. Chavez, G.E. Lienhard, and T.E. McGraw. 2007. Rab10, a target of the AS160 Rab GAP, is required for insulin-stimulated translocation of GLUT4 to the adipocyte plasma membrane. *Cell Metab*. 5:293-303.

Schutze, M.P., P.A. Peterson, and M.R. Jackson. 1994. An N-terminal double-arginine motif maintains type II membrane proteins in the endoplasmic reticulum. *EMBO J*. 13:1696-1705.

Shewan, A.M., E.M. van Dam, S. Martin, T.B. Luen, W. Hong, N.J. Bryant, and D.E. James. 2003. GLUT4 recycles via a trans-Golgi network (TGN) subdomain enriched in Syntaxins 6 and 16 but not TGN38: involvement of an acidic targeting motif. *Mol Biol Cell*. 14:973-986.

Shi, J., G. Huang, and K.V. Kandror. 2008. Self-assembly of Glut4 storage vesicles during differentiation of 3T3-L1 adipocytes. *J Biol Chem*. 283:30311-30321.

Shi, J., and K.V. Kandror. 2005. Sortilin is essential and sufficient for the formation of Glut4 storage vesicles in 3T3-L1 adipocytes. *Dev Cell*. 9:99-108.

Shi, J., and K.V. Kandror. 2007. The luminal Vps10p domain of sortilin plays the predominant role in targeting to insulin-responsive Glut4-containing vesicles. *J Biol Chem*. 282:9008-9016.

Sohda, M., Y. Misumi, S. Yoshimura, N. Nakamura, T. Fusano, S. Ogata, S. Sakisaka, and Y. Ikehara. 2007. The interaction of two tethering factors, p115 and COG complex, is required for Golgi integrity. *Traffic*. 8:270-284.

Tokumitsu, S., and W.H. Fishman. 1983. Alkaline phosphatase biosynthesis in the endoplasmic reticulum and its transport through the Golgi apparatus to the plasma membrane: cytochemical evidence. *J Histochem Cytochem*. 31:647-655.

Treacy-Abarca, S., and S. Mukherjee. 2015. Legionella suppresses the host unfolded protein response via multiple mechanisms. *Nat Commun*. 6:7887.

Trefely, S., P.S. Khoo, J.R. Krycer, R. Chaudhuri, D.J. Fazakerley, B.L. Parker, G. Sultani, J. Lee, J.P. Stephan, E. Torres, K. Jung, C. Kuijl, D.E. James, J.R. Junutula, and J. Stockli. 2015. Kinome Screen Identifies PFKFB3 and Glucose Metabolism as Important Regulators of the Insulin/Insulin-like Growth Factor (IGF)-1 Signaling Pathway. *J Biol Chem*. 290:25834-25846.

van Zuylen, W.J., P. Doyon, J.F. Clement, K.A. Khan, L.M. D'Ambrosio, F. Do, M. St-Amant-Verret, T. Wissanji, G. Emery, A.C. Gingras, S. Meloche, and M.J. Servant. 2012. Proteomic profiling of the TRAF3 interactome network reveals a new role for the ER-to-Golgi transport compartments in innate immunity. *PLoS Pathog*. 8:e1002747.

Vassilopoulos, S., C. Esk, S. Hoshino, B.H. Funke, C.Y. Chen, A.M. Plocik, W.E. Wright, R. Kucherlapati, and F.M. Brodsky. 2009. A role for the CHC22 clathrin heavy-chain isoform in human glucose metabolism. *Science*. 324:1192-1196.

Wakeham, D.E., L. Abi-Rached, M.C. Towler, J.D. Wilbur, P. Parham, and F.M. Brodsky. 2005. Clathrin heavy and light chain isoforms originated by independent mechanisms of gene duplication during chordate evolution. *Proc Natl Acad Sci U S A*. 102:7209-7214.

Waters, M.G., D.O. Clary, and J.E. Rothman. 1992. A novel 115-kD peripheral membrane protein is required for intercisternal transport in the Golgi stack. *J Cell Biol*. 118:1015-1026.

Watson, R.T., A.H. Khan, M. Furukawa, J.C. Hou, L. Li, M. Kanzaki, S. Okada, K.V. Kandror, and J.E. Pessin. 2004. Entry of newly synthesized GLUT4 into the insulin-responsive storage compartment is GGA dependent. *EMBO J*. 23:2059-2070.

Zhu, C.H., V. Mouly, R.N. Cooper, K. Mamchaoui, A. Bigot, J.W. Shay, J.P. Di Santo, G.S. Butler-Browne, and W.E. Wright. 2007. Cellular senescence in human myoblasts is overcome by human telomerase reverse transcriptase and cyclin-dependent kinase 4: consequences in aging muscle and therapeutic strategies for muscular dystrophies. *Aging Cell*. 6:515-523.

Zuckman, D.M., J.B. Hung, and C.R. Roy. 1999. Pore-forming activity is not sufficient for Legionella pneumophila phagosome trafficking and intracellular growth. *Mol Microbiol*. 32:990-1001.

Figure 1

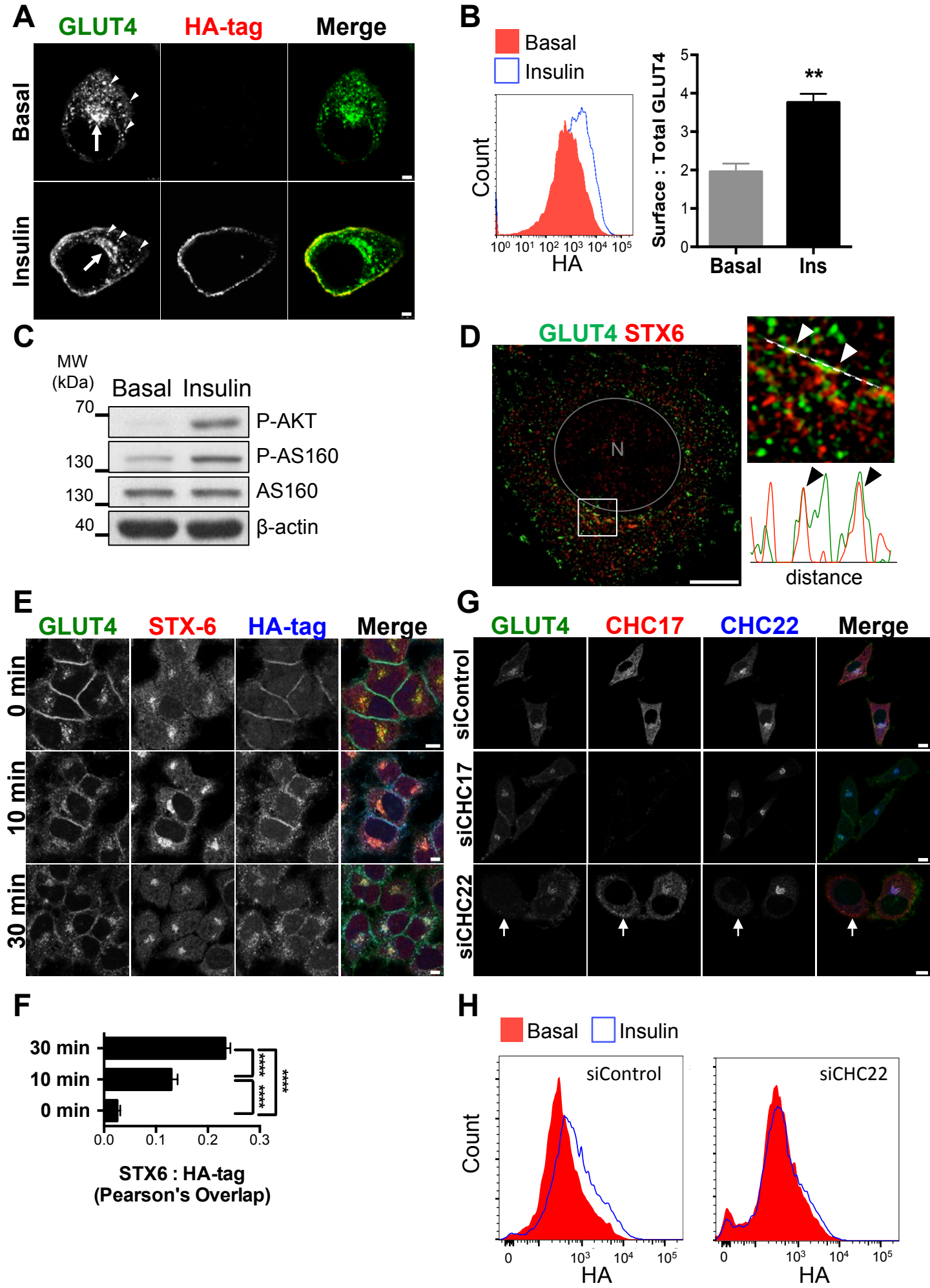
A
GLUT4
HA-tag
Merge
Basal
Insulin
B
Basal
Insulin
Count
HA
Surface : Total GLUT4
**
Basal
Ins
C
MW (kDa)
Basal
Insulin
70
P-AKT
130
P-AS160
130
AS160
40
β-actin
D
GLUT4 STX6
N
distance
E
GLUT4
STX-6
HA-tag
Merge
0 min
10 min
30 min
G
GLUT4
CHC17
CHC22
Merge
siControl
siCHC17
siCHC22
F
30 min
10 min
0 min
****
****
****
0.0
0.1
0.2
0.3
STX6 : HA-tag
(Pearson's Overlap)
H
Basal
Insulin
siControl
siCHC22
Count
HA
HA

Figure 2

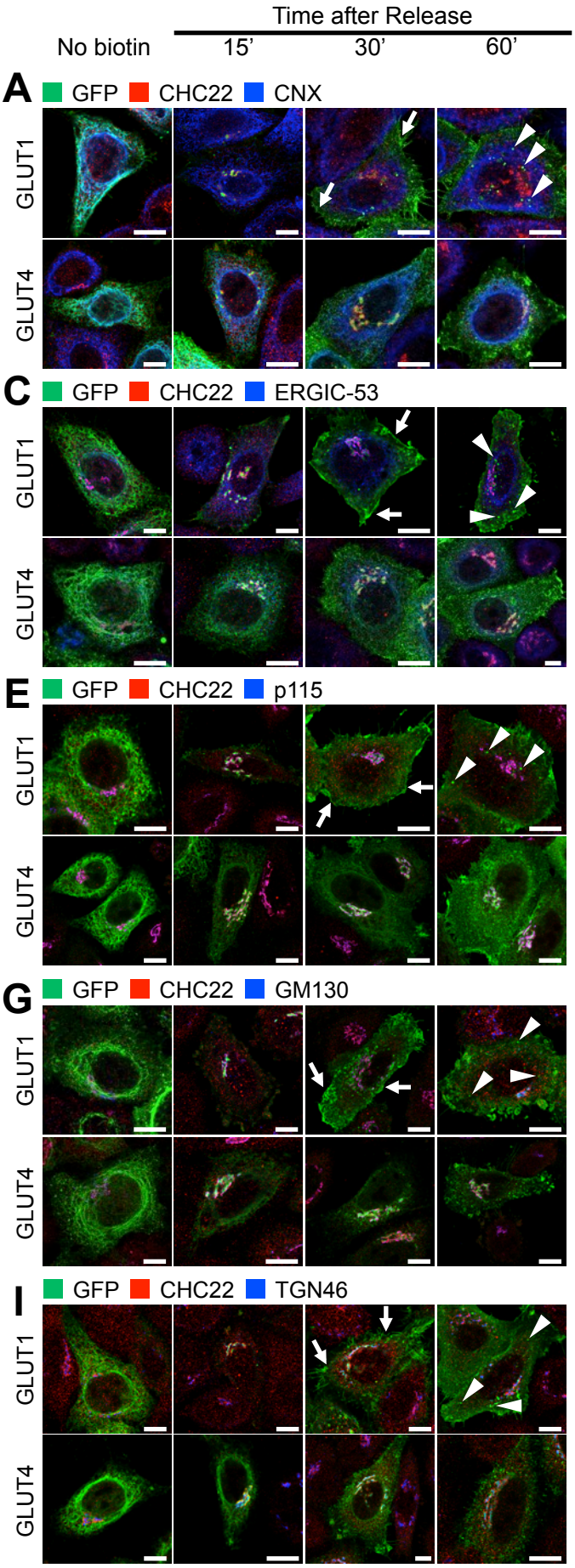
Time after Release
No biotin
15'
30'
60'
A
GFP
CHC22
CNX
GLUT1
GLUT4
C
GFP
CHC22
ERGIC-53
GLUT1
GLUT4
E
GFP
CHC22
p115
GLUT1
GLUT4
G
GFP
CHC22
GM130
GLUT1
GLUT4
I
GFP
CHC22
TGN46
GLUT1
GLUT4

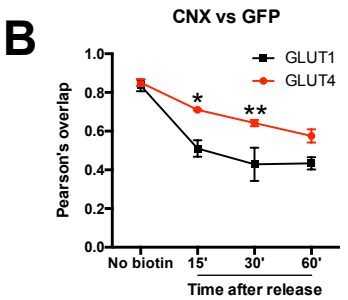
B
CNX vs GFP
GLUT1
GLUT4
Pearson's overlap
1.0
0.8
0.6
0.4
0.2
0.0
*
**
No biotin
15'
30'
60'
Time after release

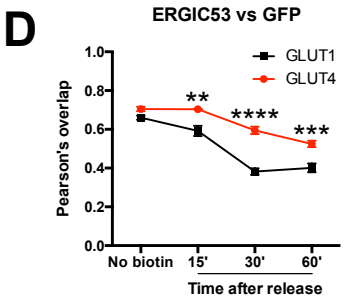
D
ERGIC53 vs GFP
GLUT1
GLUT4
Pearson's overlap
1.0
0.8
0.6
0.4
0.2
0.0
**
****
***
No biotin
15'
30'
60'
Time after release

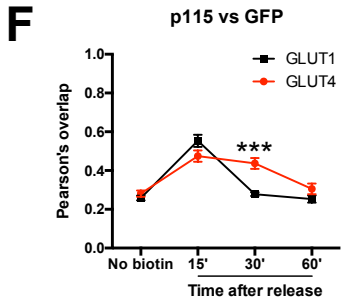
F
p115 vs GFP
GLUT1
GLUT4
Pearson's overlap
1.0
0.8
0.6
0.4
0.2
0.0
***
No biotin
15'
30'
60'
Time after release

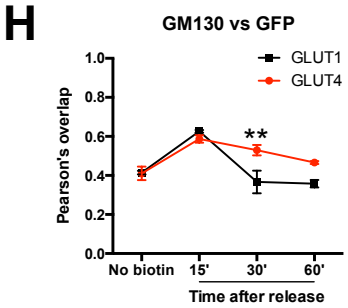
H
GM130 vs GFP
GLUT1
GLUT4
Pearson's overlap
1.0
0.8
0.6
0.4
0.2
0.0
**
No biotin
15'
30'
60'
Time after release

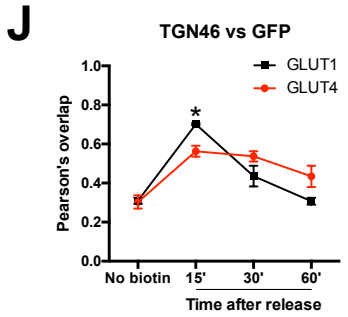
J
TGN46 vs GFP
GLUT1
GLUT4
Pearson's overlap
1.0
0.8
0.6
0.4
0.2
0.0
*
No biotin
15'
30'
60'
Time after release

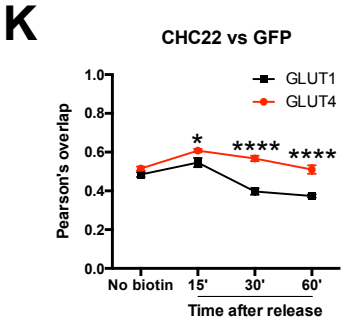
K
CHC22 vs GFP
GLUT1
GLUT4
Pearson's overlap
1.0
0.8
0.6
0.4
0.2
0.0
*
****
****
No biotin
15'
30'
60'
Time after release

Figure 3

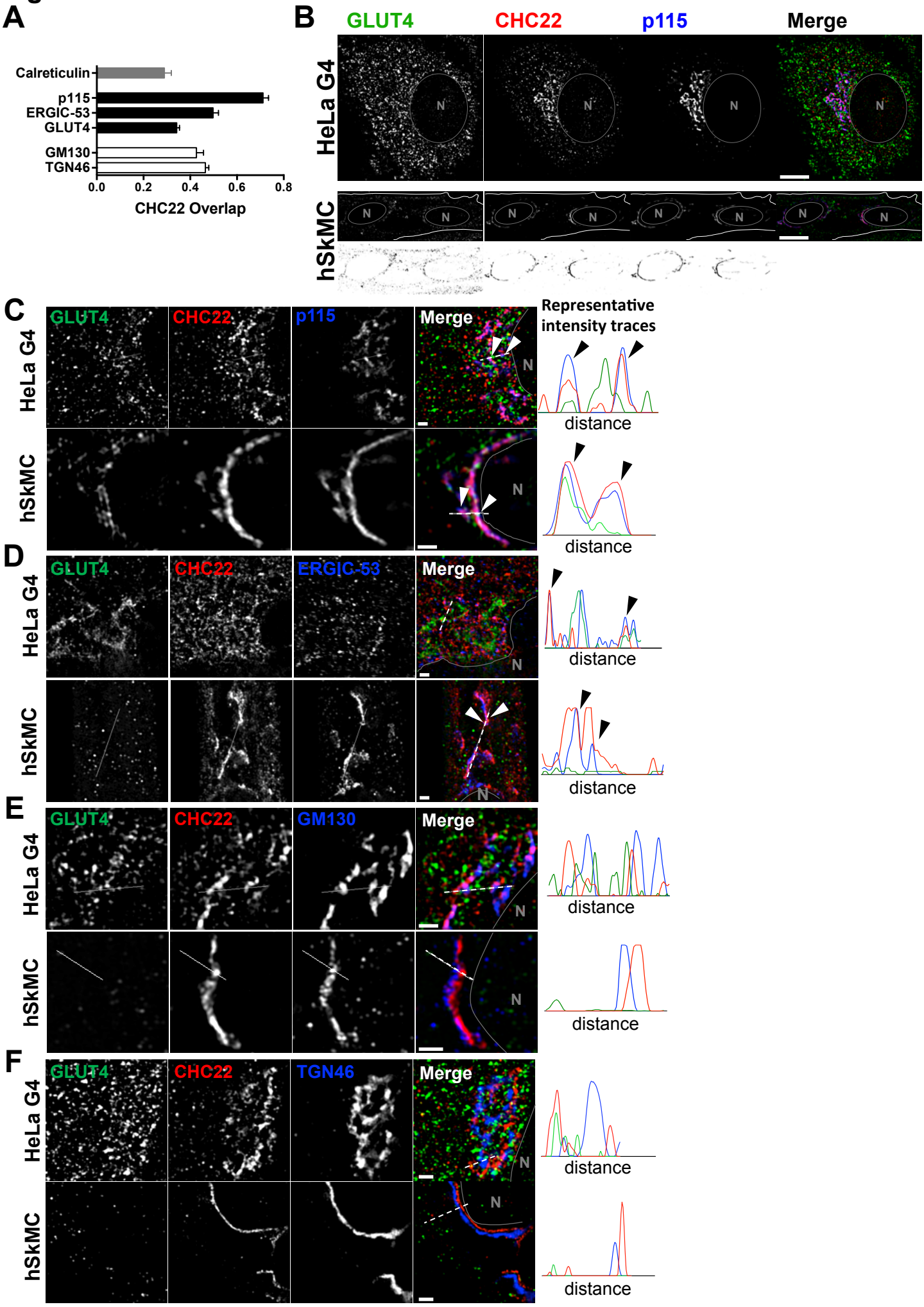
A
Calreticulin
p115
ERGIC-53
GLUT4
GM130
TGN46
0.0
0.2
0.4
0.6
0.8
CHC22 Overlap
B
GLUT4
CHC22
p115
Merge
HeLa G4
hSkMC
N
C
GLUT4
CHC22
p115
Merge
Representative intensity traces
distance
D
GLUT4
CHC22
ERGIC-53
Merge
E
GLUT4
CHC22
GM130
Merge
F
GLUT4
CHC22
TGN46
Merge

Figure 4

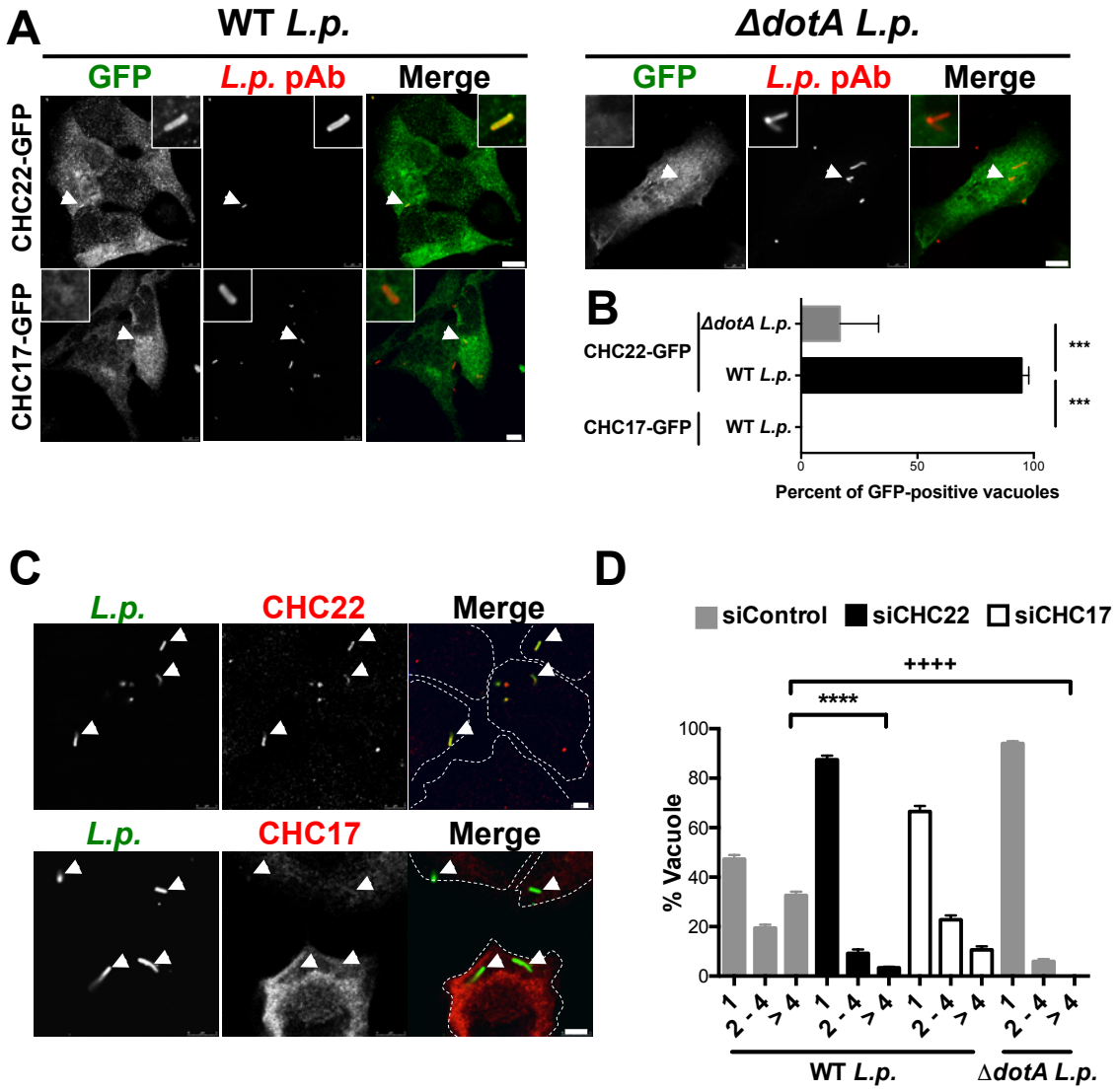
A
WT L.p.
ΔdotA L.p.
GFP
L.p. pAb
Merge
CHC22-GFP
CHC17-GFP
B
ΔdotA L.p.
WT L.p.
CHC22-GFP
CHC17-GFP
***
***
0
50
100
Percent of GFP-positive vacuoles
C
L.p.
CHC22
Merge
L.p.
CHC17
Merge
D
siControl
siCHC22
siCHC17
++++
****
% Vacuole
100
80
60
40
20
0
1
2-4
>4
WT L.p.
ΔdotA L.p.

Figure 5

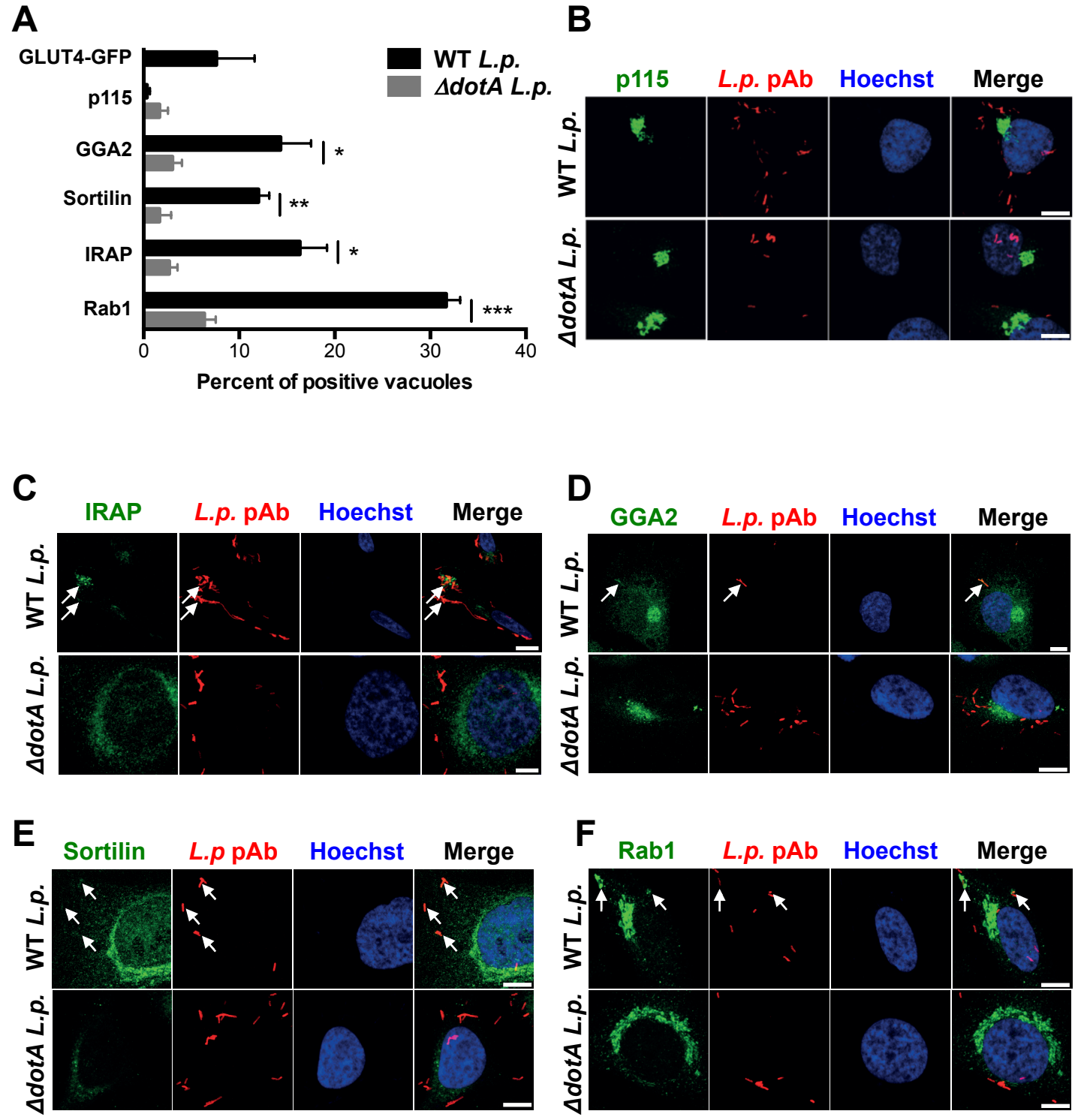
A
GLUT4-GFP
p115
GGA2
Sortilin
IRAP
Rab1
WT L.p.
ΔdotA L.p.
*
**
*
***
0
10
20
30
40
Percent of positive vacuoles
B
p115
L.p. pAb
Hoechst
Merge
WT L.p.
ΔdotA L.p.
C
IRAP
L.p. pAb
Hoechst
Merge
WT L.p.
ΔdotA L.p.
D
GGA2
L.p. pAb
Hoechst
Merge
WT L.p.
ΔdotA L.p.
E
Sortilin
L.p pAb
Hoechst
Merge
WT L.p.
ΔdotA L.p.
F
Rab1
L.p. pAb
Hoechst
Merge
WT L.p.
ΔdotA L.p.

Figure 6

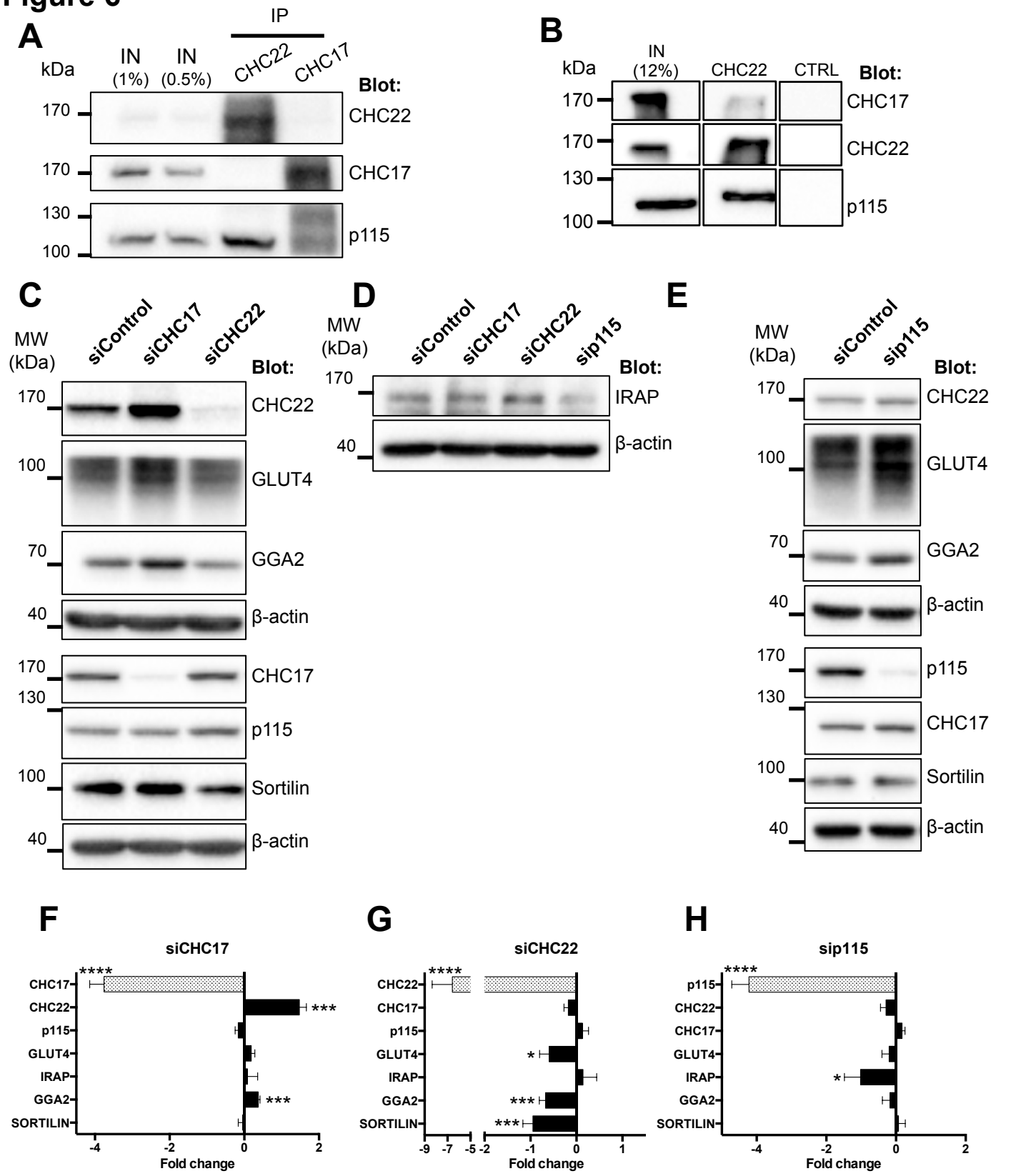
A
IP
kDa
IN (1%)
IN (0.5%)
CHC22
CHC17
Blot:
170
CHC22
170
CHC17
130
100
p115
B
kDa
IN (12%)
CHC22
CTRL
Blot:
170
CHC17
170
CHC22
130
100
p115
C
MW (kDa)
siControl
siCHC17
siCHC22
Blot:
170
CHC22
100
GLUT4
70
GGA2
40
β-actin
170
CHC17
130
p115
100
Sortilin
40
β-actin
D
MW (kDa)
siControl
siCHC17
siCHC22
sip115
Blot:
170
IRAP
40
β-actin
E
MW (kDa)
siControl
sip115
Blot:
170
CHC22
100
GLUT4
70
GGA2
40
β-actin
170
p115
130
CHC17
100
Sortilin
40
β-actin
F
siCHC17
CHC17
CHC22
p115
GLUT4
IRAP
GGA2
SORTILIN
****
***
***
-4
-2
0
2
Fold change
G
siCHC22
CHC22
CHC17
p115
GLUT4
IRAP
GGA2
SORTILIN
****
*
***
***
-9
-7
-5
-2
-1
0
1
Fold change
H
sip115
p115
CHC22
CHC17
GLUT4
IRAP
GGA2
SORTILIN
****
*
-4
-2
0
2
Fold change

Figure 7

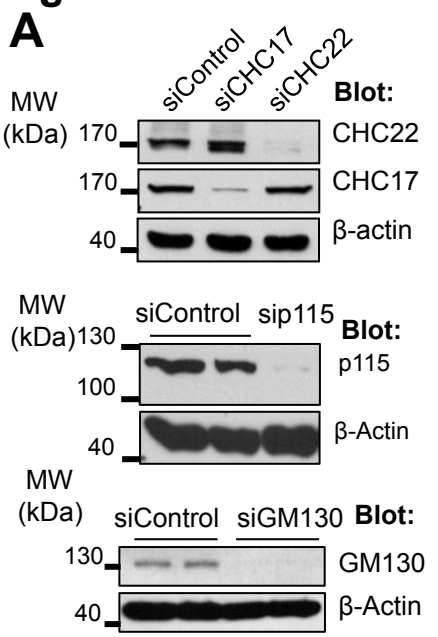
A
siControl
siCHC17
siCHC22
MW (kDa)
Blot:
170
CHC22
170
CHC17
40
β-actin
siControl
sip115
130
p115
100
β-Actin
40
siControl
siGM130
130
GM130
40
β-Actin

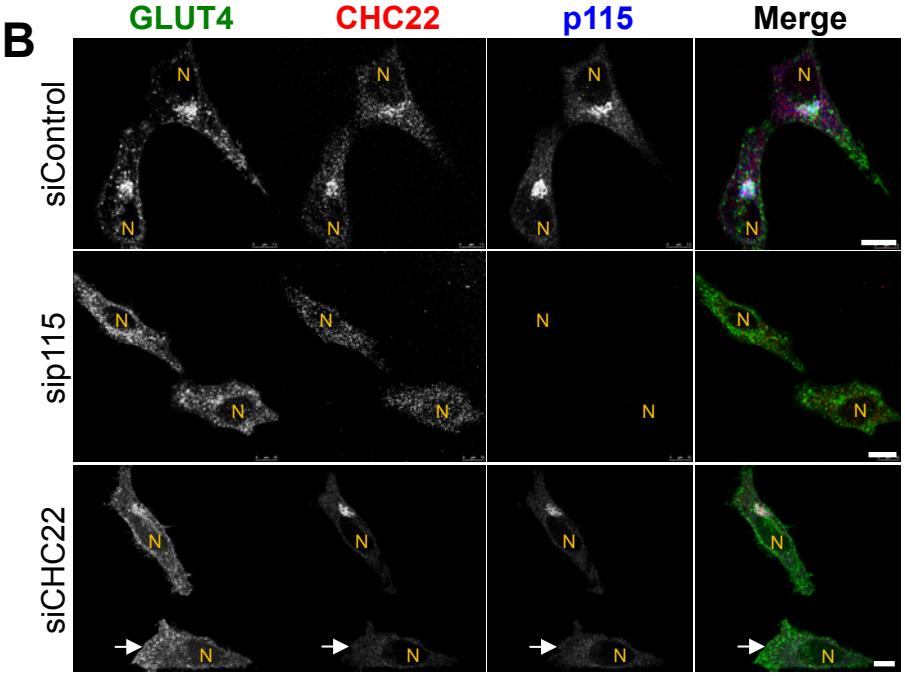
B
GLUT4
CHC22
p115
Merge
siControl
sip115
siCHC22
N

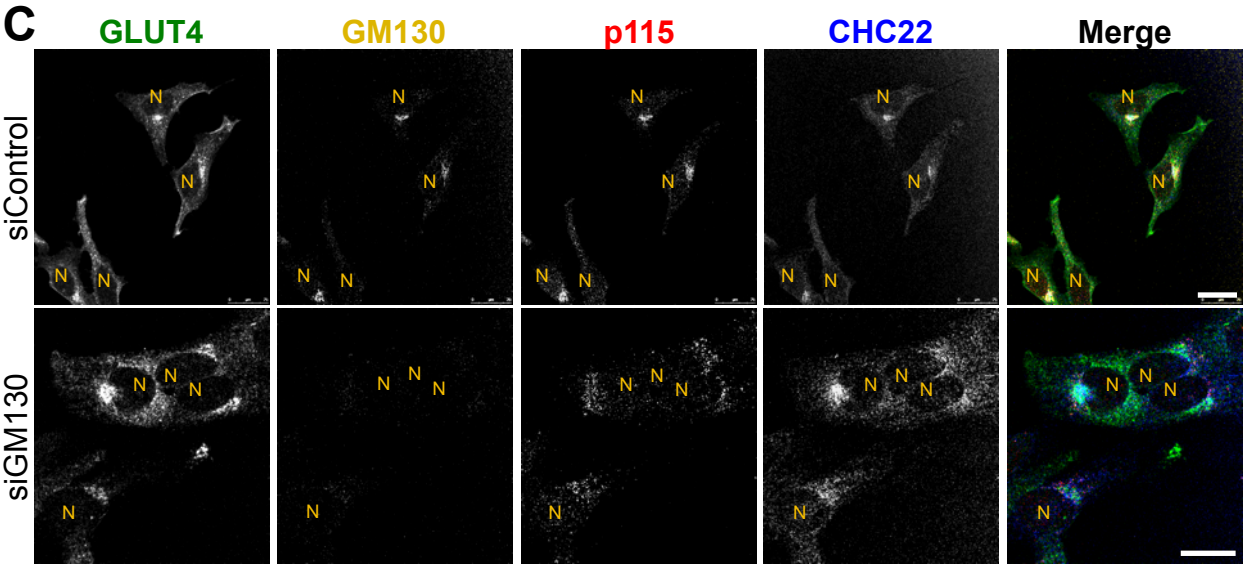
C
GLUT4
GM130
p115
CHC22
Merge
siControl
siGM130
N

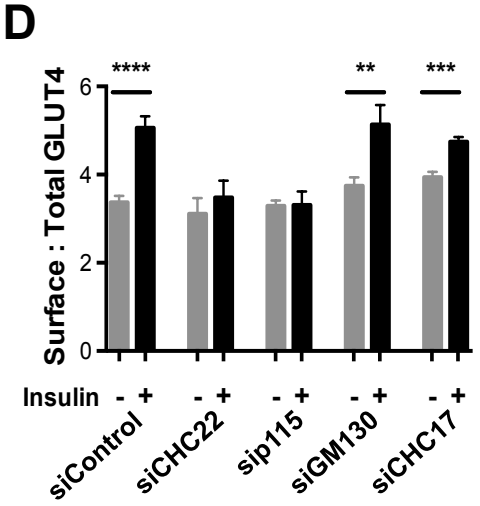
D
Surface : Total GLUT4
6
4
2
0
****
**
***
Insulin
- +
siControl
siCHC22
sip115
siGM130
siCHC17

Figure 8

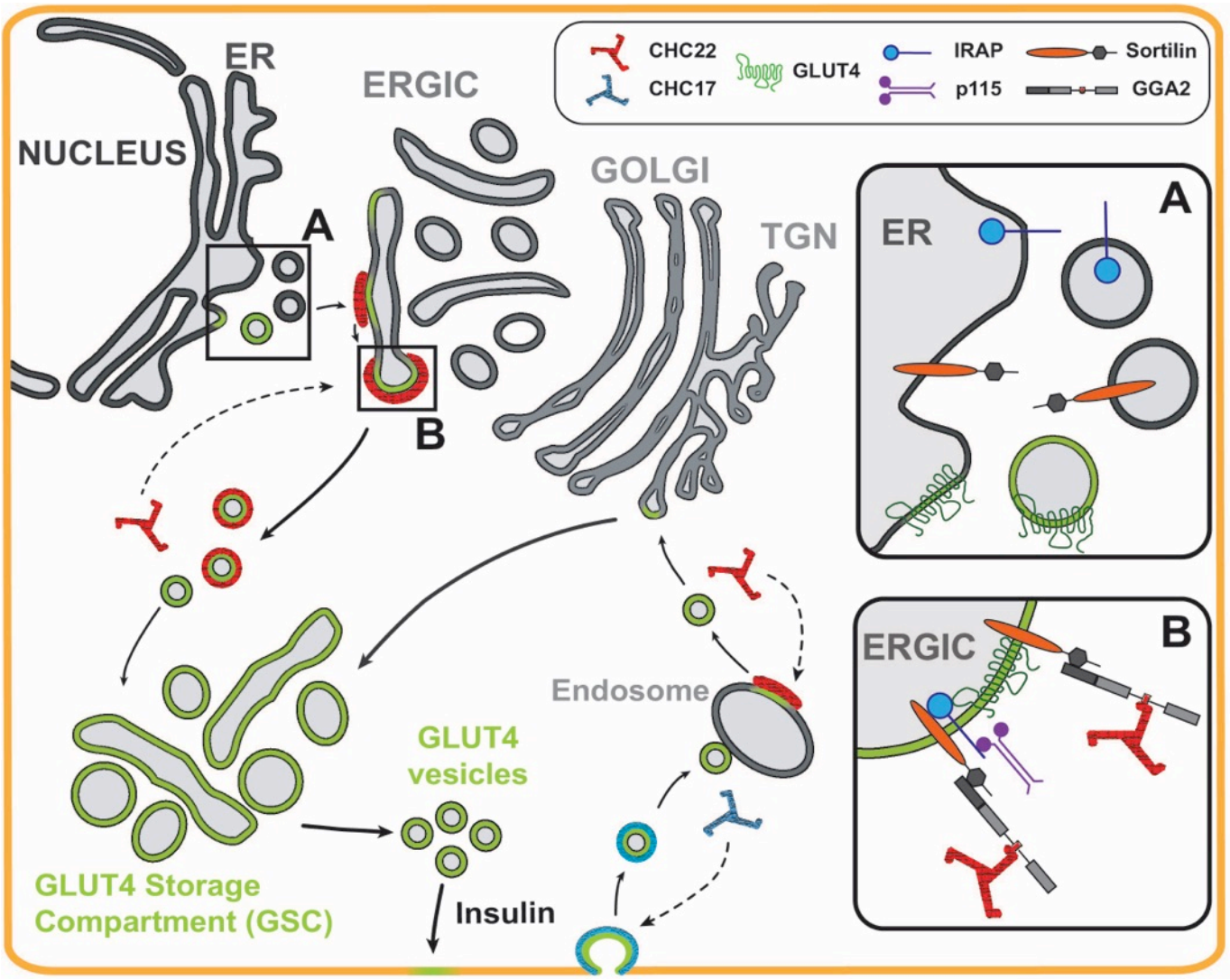
CHC22
CHC17
GLUT4
IRAP
p115
Sortilin
GGA2
ER
ERGIC
NUCLEUS
GOLGI
TGN
A
B
ER
A
ERGIC
B
Endosome
GLUT4
vesicles
GLUT4 Storage
Compartment (GSC)
Insulin

Supplemental Figures

Figure S1

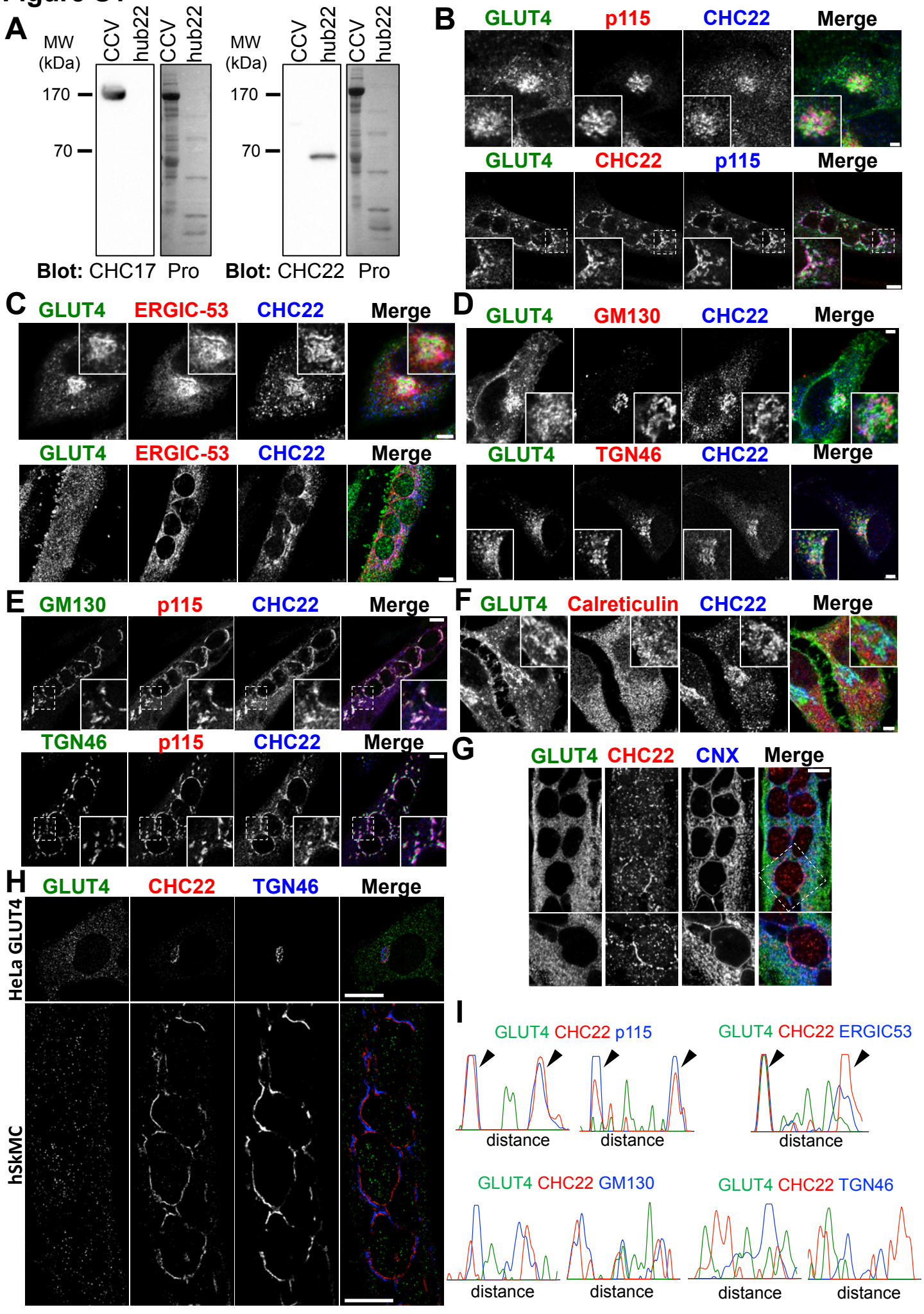
A
MW (kDa)
CCV
hub22
CCV
hub22
170
70
Blot: CHC17 Pro
MW (kDa)
CCV
hub22
CCV
hub22
170
70
Blot: CHC22 Pro
B
GLUT4
p115
CHC22
Merge
GLUT4
CHC22
p115
Merge
C
GLUT4
ERGIC-53
CHC22
Merge
GLUT4
ERGIC-53
CHC22
Merge
D
GLUT4
GM130
CHC22
Merge
GLUT4
TGN46
CHC22
Merge
E
GM130
p115
CHC22
Merge
TGN46
p115
CHC22
Merge
F
GLUT4
Calreticulin
CHC22
Merge
G
GLUT4
CHC22
CNX
Merge
H
GLUT4
CHC22
TGN46
Merge
HeLa GLUT4
hSkMC
I
GLUT4 CHC22 p115
distance
distance
GLUT4 CHC22 ERGIC53
distance
GLUT4 CHC22 GM130
distance
distance
GLUT4 CHC22 TGN46
distance
distance

Figure S2

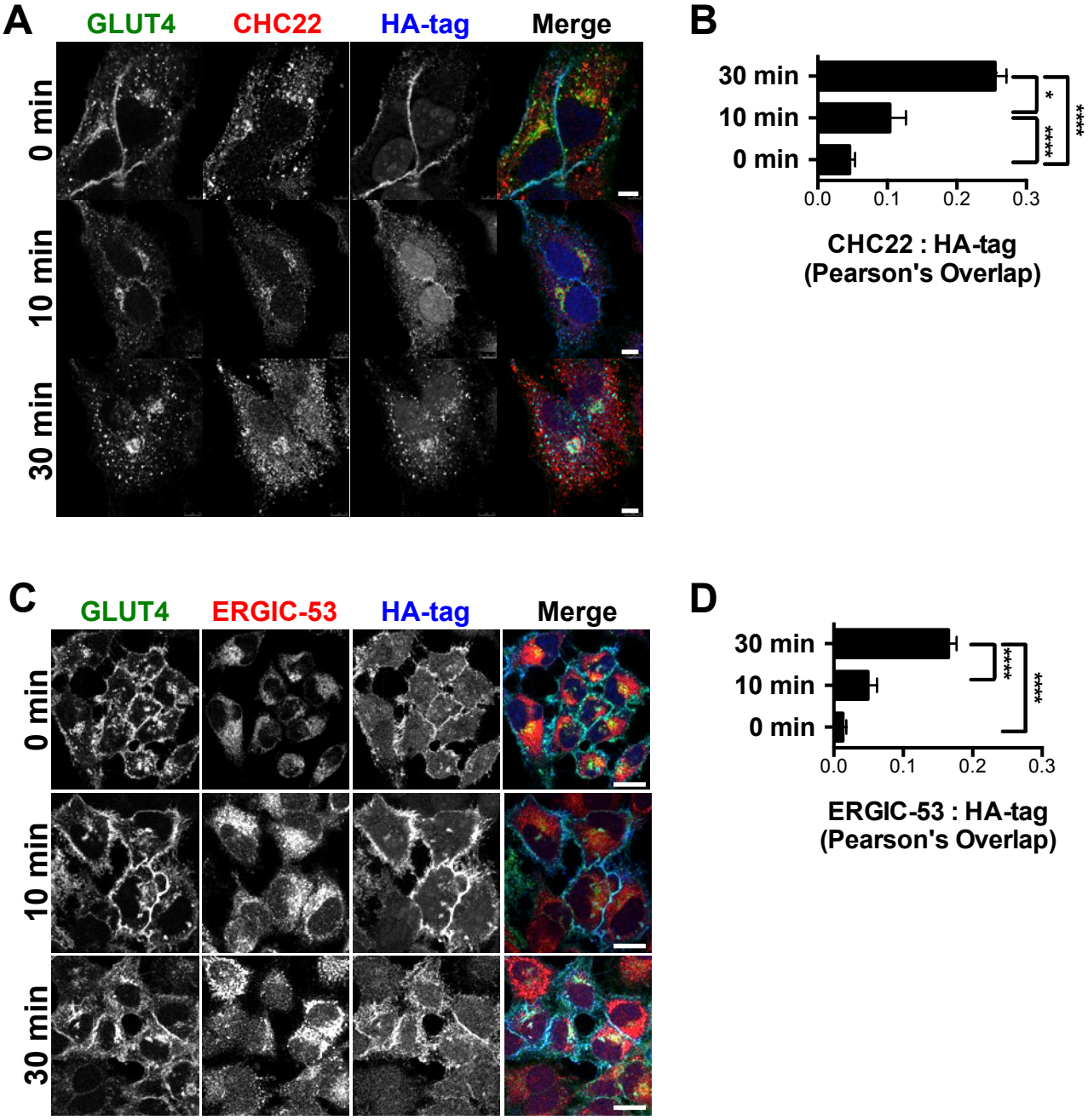
A
GLUT4
CHC22
HA-tag
Merge
0 min
10 min
30 min
B
30 min
10 min
0 min
0.0
0.1
0.2
0.3
*
****
****
CHC22 : HA-tag
(Pearson's Overlap)
C
GLUT4
ERGIC-53
HA-tag
Merge
0 min
10 min
30 min
D
30 min
10 min
0 min
0.0
0.1
0.2
0.3
****
****
ERGIC-53 : HA-tag
(Pearson's Overlap)

Figure S3

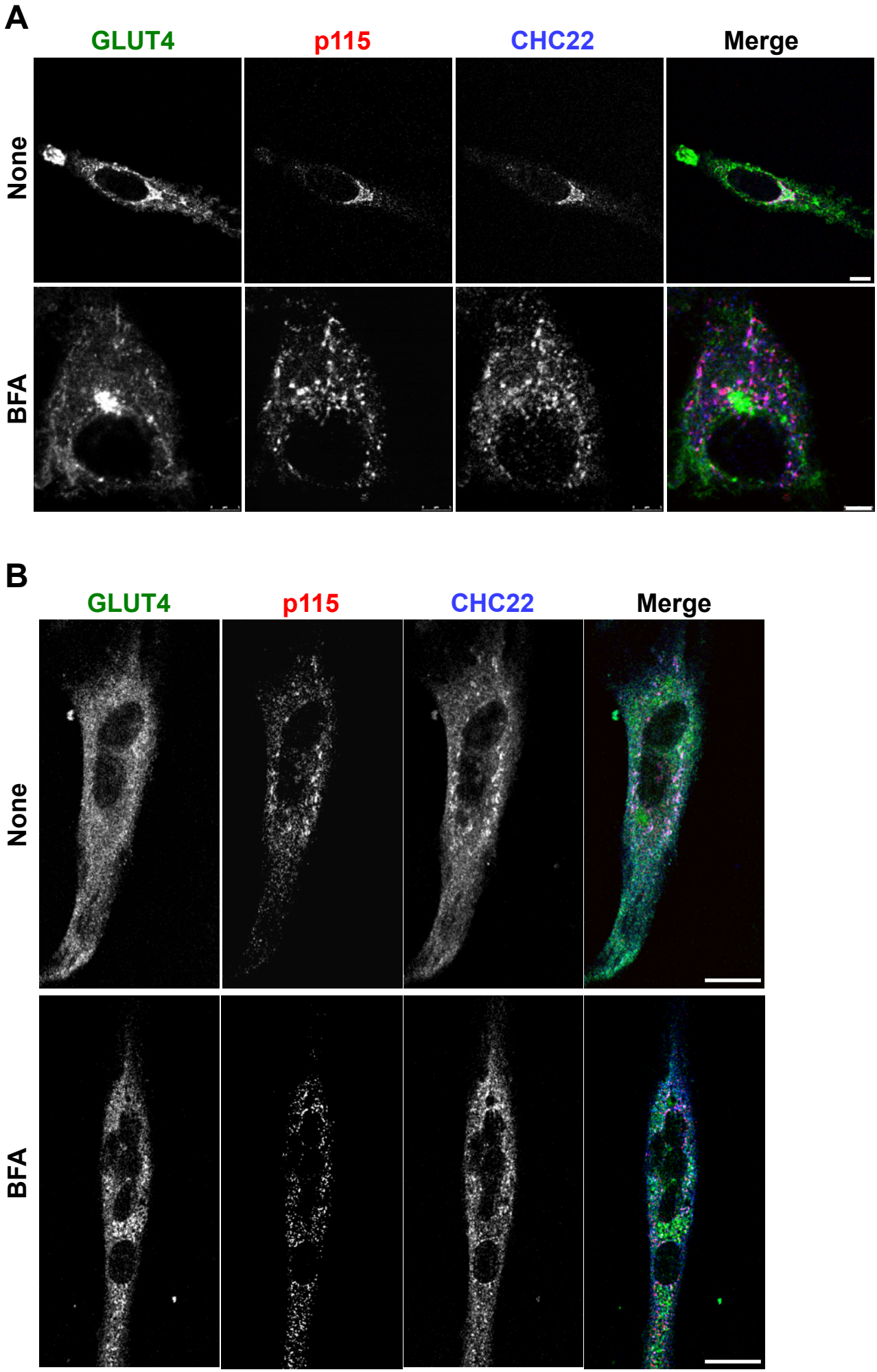
A
GLUT4
p115
CHC22
Merge
None
BFA
B
GLUT4
p115
CHC22
Merge
None
BFA

Figure S4

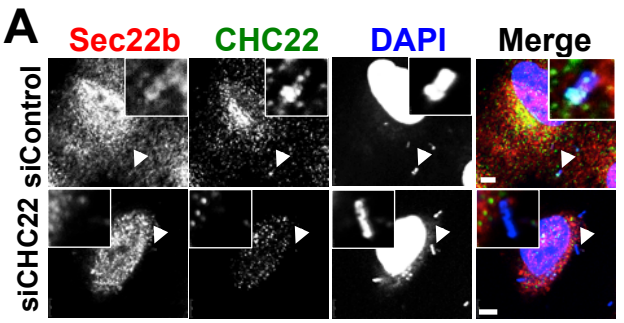
A
Sec22b
CHC22
DAPI
Merge
siControl
siCHC22

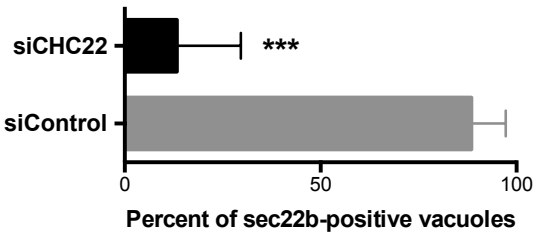
B
siCHC22
siControl
***
0
50
100
Percent of sec22b-positive vacuoles

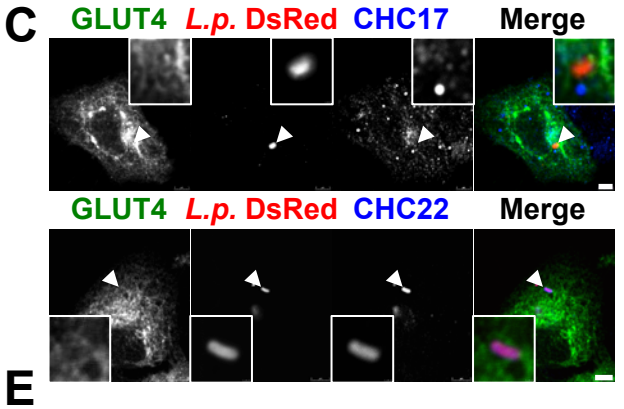
C
GLUT4
L.p. DsRed
CHC17
Merge
GLUT4
L.p. DsRed
CHC22
Merge

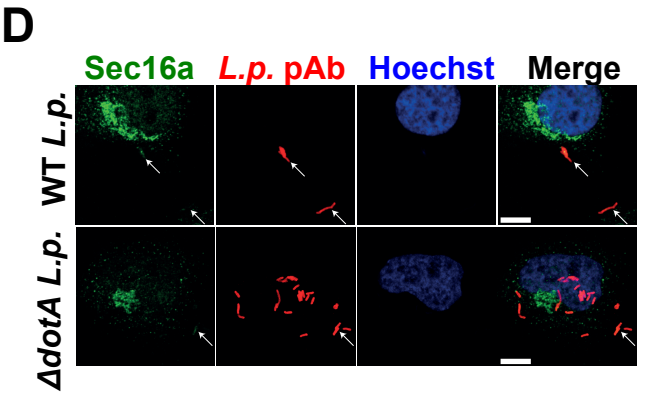
D
Sec16a
L.p. pAb
Hoechst
Merge
WT L.p.
ΔdotA L.p.

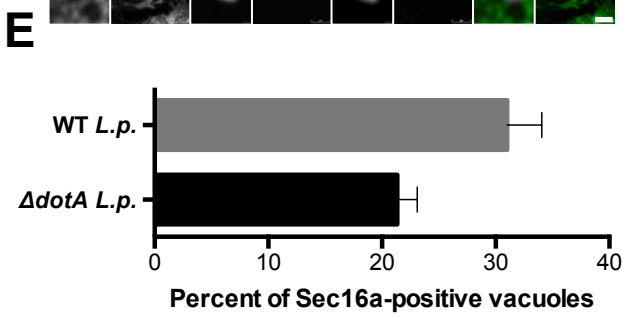
E
WT L.p.
ΔdotA L.p.
0
10
20
30
40
Percent of Sec16a-positive vacuoles

Figure S5

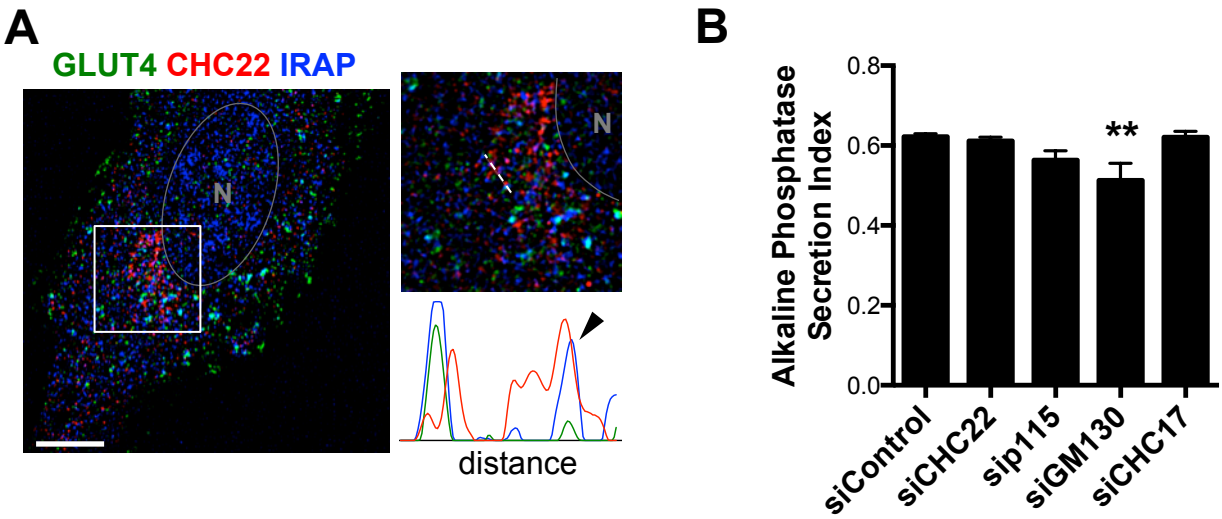
A
GLUT4 CHC22 IRAP
N
N
distance
B
Alkaline Phosphatase Secretion Index
0.8
0.6
0.4
0.2
0.0
**
siControl
siCHC22
sip115
siGM130
siCHC17